



**HAL**  
open science

## **An attempt to link suspended load hysteresis patterns and sediment sources configuration in alpine catchments**

C. Misset, A. Recking, C. Legout, A. Poirel, M. Cazilhac, M. Esteves, M. Bertrand

### ► **To cite this version:**

C. Misset, A. Recking, C. Legout, A. Poirel, M. Cazilhac, et al.. An attempt to link suspended load hysteresis patterns and sediment sources configuration in alpine catchments. *Journal of Hydrology*, 2019, 576, pp.72-84. 10.1016/j.jhydrol.2019.06.039 . hal-02610280

**HAL Id: hal-02610280**

**<https://hal.inrae.fr/hal-02610280v1>**

Submitted on 26 Oct 2021

**HAL** is a multi-disciplinary open access archive for the deposit and dissemination of scientific research documents, whether they are published or not. The documents may come from teaching and research institutions in France or abroad, or from public or private research centers.

L'archive ouverte pluridisciplinaire **HAL**, est destinée au dépôt et à la diffusion de documents scientifiques de niveau recherche, publiés ou non, émanant des établissements d'enseignement et de recherche français ou étrangers, des laboratoires publics ou privés.



Distributed under a Creative Commons Attribution - NonCommercial 4.0 International License

# 1 **AN ATTEMPT TO LINK SUSPENDED LOAD** 2 **HYSTERESIS PATTERNS AND SEDIMENT** 3 **SOURCES CONFIGURATION IN ALPINE** 4 **CATCHMENTS**

## 5 **Authors**

6 C. Misset<sup>1\*</sup>, A. Recking<sup>1</sup>, C. Legout<sup>2</sup>, A. Poirel<sup>3</sup>, M. Cazihlac<sup>3</sup>, M. Esteves<sup>2</sup>, M. Bertrand<sup>1</sup>.

7

8 <sup>1</sup> Univ. Grenoble Alpes, Irstea, ETNA, 38000 Grenoble, France

9 <sup>2</sup> Univ. Grenoble Alpes, CNRS, IRD, Grenoble INP, IGE, 38000 Grenoble, France

10 <sup>3</sup> EDF, DTG, 38100 Grenoble, France

11 \* Corresponding author

## 12 **ABSTRACT**

13 A large part of total solid flux is transported as suspension in mountainous rivers. It is  
14 crucial for water resource management and for environmental issues to be able to model  
15 and to understand these fluxes. However, suspended load is known to be highly variable  
16 in time and space, as fine sediments can originate from various erosion processes and  
17 from various sources. Among the different methodologies available for analyzing the  
18 suspended sediment flux dynamics, hysteretic loops in discharge and suspended load  
19 signals are commonly used to assess sediment sources and production processes.  
20 However, the shape of these loops is often analyzed qualitatively for a single or a small  
21 number of catchments. Hence it is still unclear how the geomorphological catchment  
22 properties influence the variability of the flow rate - suspended sediment concentration

23 relationship through the hysteresis effects. This is particularly true in mountainous  
24 catchments where important sources of fine sediments may originate from the river bed  
25 in addition to hillslopes.

26 In this study we analyzed quantitatively ten long-term series of high-frequency  
27 observations of suspended sediment load measured in contrasted alpine catchments.  
28 Hysteresis effects were analyzed in a high number of automated sampled events and  
29 the dominant response for each catchment was sought. This was done by using a  
30 normalized hysteresis index developed by Lloyd et al. (2016), which we weighted by the  
31 mass transported during each event. The various catchments were characterized with a  
32 normalized geomorphological index expressing the relative importance of sediment  
33 sources originating from the river bed or from eroded areas as a function of the distance  
34 to the outlet of the catchment.

35 The dominant hysteresis response of the ten alpine catchments studied was found to be  
36 greatly linked to their geomorphological index. These results suggest that the sediment  
37 source configuration upstream of a measuring station drive hysteresis effects and thus  
38 the variability of the flow rate-suspended sediment concentration relationship.

39 Keywords: Suspended load, hysteresis, sediment sources, alpine catchments

## 40 1. INTRODUCTION

41 Suspended sediment load (SSL) assessment is essential for water resource  
42 management and for many environmental issues. Whereas fine sediments transported  
43 by rivers are a vector of nutrients that are essential for estuarine ecosystems [*Le Pape*  
44 *et al.*, 2013; *Ludwig and Probst*, 1998], they are also associated with socio-economic  
45 issues due to reservoir siltation or contaminant transport [*Vercauysse et al.*, 2017;  
46 *Walling et al.*, 2003].

47 SSL is known to be highly variable in time and space especially in mountainous areas  
48 given that fine sediments can originate either from the main fluvial system or from  
49 external sources in similar proportions [*Guillon et al.*, 2018; *Navratil et al.*, 2010; *Orwin*  
50 *and Smart*, 2004]. According to the concept proposed by Bogen (1980) and the  
51 conceptual models used by Picouet (2009) or Park and Hunt (2017), the first type of  
52 production consists of sediment resuspension from the river bed. This part of  
53 suspension is believed to be related to flow rate, shear stress, or stream power [*Park*  
54 *and Hunt*, 2017]. In this case, fine sediments are produced by resuspension of deposited  
55 fine particles on bars, in secondary channels, when the armor layer is mobilized [*Navratil*  
56 *et al.*, 2010] or when bank erosion occurs [*Lefrançois et al.*, 2007]. The second type  
57 concerns erosion processes that take place in the catchment and that may not be  
58 directly related to the flow rate measured in the main channel. Fine particles are  
59 produced by rainfall or runoff detachment on eroded areas, in first-order tributaries or by  
60 mass movement.

61 The coexistence of these two kinds of fine sediment production processes often  
62 generates a huge variability in the flow rate (Q)–suspended sediment concentration  
63 (SSC) relationship. As observed in many field studies at the event, inter-event, or  
64 seasonal time scale, the same flow solicitation does not lead to the same sediment  
65 response of the watershed [*Aich et al.*, 2014; *Andermann et al.*, 2012; *Mao and Carrillo*,  
66 2016; *Sun et al.*, 2016]. This non-unique relation between Q and SSC is often  
67 highlighted through hysteresis loop observations. These phenomena have been widely  
68 analyzed in the past few decades and in various environments [*Aguilera and Melack*,  
69 2018; *Baca*, 2010; *Bogen*, 1980; *Gharari and Razavi*, 2018; *Klein*, 1984; *Smith and*  
70 *Dragovich*, 2009; *Tananaev*, 2015; *Zuecco et al.*, 2016]. The first classification of  
71 hysteresis loops was proposed by Williams (1989). Five classes were distinguished:  
72 single-valued line, clockwise loops, counterclockwise loops, single line plus a loop, and  
73 figure-of-eight loop. This classification was then re-used and completed with more  
74 complex figures by various authors such as Nistor and Church (2005), Tananaev (2015),  
75 Duvert *et al.* (2010) or Hamshaw *et al.* (2018). In a literature review, Gellis (2013)  
76 highlights that a given hysteresis effect observed at a measuring station can be  
77 explained by various erosion and physical processes.

78 However, at the event scale, distant sediment sources were found to generate mainly  
79 counterclockwise loops [*Baca*, 2010; *Klein*, 1984; *Williams*, 1989]. Suspended  
80 sediments are transported more or less at the mean flow velocity, which is lower than  
81 the flood wave celerity. This means that if the travelling distance and the relative  
82 difference between the celerity of the two waves is high enough, a time delay will be  
83 observed between the two signals generating a counterclockwise loop [*Klein*, 1984;

84 *Nistor and Church, 2005; Williams, 1989*]. By contrast, depletion in the SSC during the  
85 falling limb of the flood or an SSC peak prior to a Q peak will generate a clockwise loop.  
86 This is usually attributed to a mobilization of relatively close and supply limited sources  
87 [*Marttila and Kløve, 2010; Park and Hunt, 2017*], dilution due to base flow increase  
88 during the falling limb [*Baca, 2010*], or rainfall close to the catchment outlet [*Jansson,*  
89 *2002*]. Many other processes could generate hysteresis between SSC and Q such as  
90 the contribution of upstream tributaries [*Asselman, 1999*], bank erosion [*Smith and*  
91 *Dragovich, 2009*], or hysteresis effects in the SSC–turbidity calibration curve [*Landers*  
92 *and Sturm, 2013*]. In some cases, the SSC and Q curve are synchronized, leading to no  
93 hysteresis pattern. Such situations were often interpreted as an unlimited sediment  
94 supply [*Nistor and Church, 2005; Williams, 1989*]. Finally, complex patterns can be  
95 observed for multi-peak events or when several processes described previously occur at  
96 the same time in the catchment.

97 Given the high number of processes leading to Q–SSC hysteresis, it is doubtful to infer  
98 even qualitatively the major erosion processes acting in a unique catchment with this  
99 single information especially when measurements are conducted for short time periods  
100 [*Esteves et al., 2018*]. On the other hand, using measurements made on several  
101 contrasted watersheds at regional scale could help to assess to which extent the  
102 sediment sources configuration may control the shape of these hysteresis and thus to  
103 better understand the spatial variability in the Q–SSC relation. During the last decades,  
104 there has been a growing interest in sediment sources characterization [*Parsons et al.,*  
105 *2015; Wohl, 2017*] as sediment contributing areas have been shown to control sediment  
106 yield in alpine catchments [*de Vente et al., 2006; Haas et al., 2011*]. Despite the

107 respective contribution of each sediment sources are often highly variable in time and  
108 space [*Legout et al.*, 2013], several methods have been proposed to quantify sediment  
109 connectivity in catchments [*Borselli et al.*, 2008; *Heckmann et al.*, 2018; *Heckmann and*  
110 *Schwanghart*, 2013]. Most of these methods conceptually consider an upslope  
111 (contributing area) and a downslope (source to sink) component to spatially describe the  
112 capacity of the catchment to export sediments [*Borselli et al.*, 2008; *Cavalli et al.*, 2013;  
113 *Heckmann and Schwanghart*, 2013]. While this separation in two components in  
114 connectivity indexes (i.e. upslope and downslope) is similar to the conceptual distinction  
115 in two sediment sources (hillslope vs riverbed production) often depicted as the main  
116 controlling factor of discharge-suspended sediment concentration hysteresis, no study  
117 reported any attempt to quantify the potential links between hysteresis and conceptual  
118 description of sediment sources.

119 This study attempts to fill this gap by analyzing long-term series with high-frequency  
120 observations of SSL made in ten contrasted mountainous catchments in the French  
121 Alps. The main objectives were (i) to describe the dominant hysteresis patterns, (ii) to  
122 propose a method describing fine sediment source configuration at the catchment scale,  
123 and (iii) to analyze the link between dominant hysteresis patterns and sediment source  
124 configuration.

## 125 2. MATERIAL AND METHODS

### 126 2.1. HYDRO-GEOMORPHOLOGICAL CHARACTERISTICS OF THE 127 CATCHMENTS

128 Four of the ten catchments studied (Asse, Bléone, Galabre, and Bès) are located in the  
129 southern part of the French Alps, and four others (Romanche, Arvan, Glandon, and Arc)  
130 are in the northern part (Figure 1). Two basins (Drac and Buëch) have intermediate  
131 positions. The ten catchments belong to the long-term observatory networks of two  
132 French research infrastructures (OZCAR and RZA) or from the monitoring network of  
133 Electricité de France Company (EDF).

134 **Figure 1**

### 135 *2.1.1. SPATIAL INFORMATION USED*

136 Data were collected for several characteristics of the basins (Table 1). Monthly average  
137 specific discharges were obtained from the French hydrometric agency (Banque Hydro:  
138 <http://www.hydro.eaufrance.fr/>) whereas spatial catchment properties were obtained  
139 thanks to a GIS analysis of several spatial databases (BD ORTHO®, BD ALTI®, Corine  
140 Land Cover®, GeoFLA®, IGN©). Active channel widths were digitalized manually on  
141 aerial orthophotographies and the fluvial corridor tool box [*Roux et al., 2015*] was used in  
142 ARCGIS 10.3 to extract the active channel width at a regular step of 20 m. The median  
143 active river bed width calculated over the first 10 km upstream the station ( $W_{10}$ ). The  
144 mean riverbed slope was obtained from the French National Institute of Geography  
145 website (<https://geodesie.ign.fr/fiches/>) for approximately 10 km upstream of each  
146 measuring station ( $S_{10}$ ). A georeferenced dataset of polygonal features with the location  
147 of eroded areas in the Alps (<https://journals.openedition.org/rga/3543#tocto2n6>) was  
148 used for the Bléone, Asse, Bès, Galabre, Buëch, Drac, and Romanche catchments  
149 [*Bertrand, 2014; Bertrand et al., 2017*]. These areas can be easily recognized in alpine  
150 catchments on high-resolution orthophotos and manually digitized using classic GIS



151 toolkits or using automatic extraction procedure as it have been done in several  
152 previous studies [*Marden et al.*, 2005; *Trustrum and Stephens*, 1981; *Vrieling*, 2006].  
153 Bertrand et al. (2017) obtained the eroded patches map used in this study by combining  
154 object-based supervised classification models on infrared aerial orthophotographies  
155 (831 tiles, 0.5 m resolution) and a pixel-based supervised classification model on  
156 Landsat 7 ETM+ images (three images, with 30 m resolution and offering a wider  
157 spectral range than aerial orthophotographies) to extract eroded areas in the southern  
158 part of the Alps. The training and validation datasets used are each constituted of 30  
159 infrared aerial orthophotographies tiles (randomly sampled in the 831 tiles) automatically  
160 segmented into objects having homogeneous textures and manually classified into two  
161 categories: eroded areas and non-eroded areas. The final classification model is a  
162 weighted sum of these calibrated models (both object-based and pixel-based). They  
163 obtained a model sensitivity, specificity and overall classification score of respectively  
164 0.81, 0.94 and 0.9. They also performed an expert classification on 500 randomly  
165 distributed points in the Bléone catchment and obtained similar results (0.74, 0.99 and  
166 0.96 respectively) confirming the reliability of this method. For the Glandon, Arvan, and  
167 Arc basins, this map was not available and eroded areas were digitalized manually using  
168 50-cm resolution aerial orthophotographies. In both cases, eroded patches are  
169 considered through the image analysis as exposed and unvegetated areas exhibiting  
170 erosion patterns or gullies. This eroded areas description is consistent with the fact that  
171 increasing bare soils cover increases suspended sediment yield [*Douglas*, 1967; *Duvert*  
172 *et al.*, 2012].

### 173 2.1.2. HYDROLOGICAL REGIMES

174 Table 1 shows the contrasting characteristics of the ten catchments. Their areas range  
175 from 22 km<sup>2</sup> to nearly 900 km<sup>2</sup>. The hydrology of the catchments located in the Southern  
176 Alps, including the Buëch basin, exhibits a high-flow period in winter and late autumn,  
177 separated by a low-flow period in summer (Figure 2). The northern catchments have  
178 higher specific water discharges. They are characterized by the presence of snow cover  
179 and glaciers resulting in a melting season generating high flows from late spring to mid-  
180 summer and low-flow periods the rest of the time. The Drac catchment exhibits an  
181 intermediate discharge regime with a melting season in late spring followed by low-flow  
182 period in summer and another high-flow period in autumn due to widespread rainfall  
183 events. The northern catchments are higher in altitude (61% of mean area above 2,000  
184 m) than southern ones (98% of mean area under 2,000 m), with the Drac exhibiting an  
185 intermediate situation (35% of catchment area above 2,000 m).

### 186 *2.1.3. GEOMORPHOLOGICAL CHARACTERISTICS*

187 Various land cover and lithologies are present on these catchments. Northern  
188 catchments, including the Drac basin, have large areas prone to erosion with zones  
189 having no or low vegetation cover ranging from 24% to 51% of their total area and rocks  
190 considered as non-resistant covering between 57% and 99% of their area. The Arvan,  
191 Glandon and Romanche catchments comprise mainly narrow mountain valleys with  
192 laterally constrained streams. Few alluvial reaches are included in the dominant step-  
193 pool sections with mean river bed slopes on the first 10 km upstream the station ( $S_{10}$ )  
194 comprised between 4% and 5.9% and median river bed active widths on the first 10 km  
195 upstream the station ( $W_{10}$ ) ranging between 8m and 22m. Having a larger catchment  
196 area, the Arc has a gentler river bed slope ( $S_{10}=1.12\%$ ) and a wider river bed active  
197 width ( $W_{10}=33m$ ). It exhibits mainly plan bed sections with few gavel bars downstream

198 active tributaries punctuated with narrow gorge sections. The Drac basin has poorly  
199 laterally constrained streams in its downstream part and a gentle slope ( $S_{10}=1.01\%$ )  
200 enabling the development of braiding sections on dozen of kilometers ( $W_{10}=60\text{m}$ ).  
201 Southern catchments, including the Buëch basin are also prone to erosion with a fraction  
202 of their basin that has low or no vegetation cover ranging between 10% and 19% and  
203 non-resistant rocks cover ranging between 79% and 100%. Their valleys are wider than  
204 the northern catchments except for the Galabre catchment which is a small headwater  
205 stream ( $A=22\text{km}^2$ ) with constrained gorges and step-pool sections ( $W_{10}=8\text{m}$ ,  $S_{10}=8.8\%$ ).  
206 The Bléone and Buëch exhibit braiding morphologies ( $W_{10}$  of respectively 162m and  
207 118m) with gentle slopes ( $S_{10}$  of respectively 0.82% and 0.81%). The Asse and Bès  
208 catchments also exhibit long alluvial and gentle sections which are punctuated with  
209 narrower sections in gorges or more constrained valleys ( $W_{10}$  of respectively 28m and  
210 20m,  $S_{10}$  of respectively 0.87% and 2.57%). Mano *et al.* (2009) reported specific  
211 suspended sediment fluxes around  $500 \text{ t km}^{-2} \text{ year}^{-1}$  for the Asse, Bléone and  
212 Romanche catchment while Navratil *et al.* (2012) reported specific suspended sediment  
213 fluxes of respectively 330, 690, and  $680 \text{ t km}^{-2} \text{ year}^{-1}$  for the Bléone, Bès and Galabre  
214 basins which can be classified as high according to the classification proposed by  
215 Meybec *et al.* (2003). These studies suggest that the studied catchments have highly  
216 active fine sediment sources. Also, all of these catchments have been chosen for their  
217 limited human impact, i.e. with limited presence of embankments or weirs in the rivers,  
218 limited urbanized areas and absence of large dams. Few small water intakes with limited  
219 storage capacity are however present (Glandon, Arvan, Drac, Romanche and Arc  
220 basins) but can be considered to have a negligible effect on the downstream suspended  
221 load transfer during the studied flood events.

222 **Figure 2**

223 **Table 1**

## 224 2.2. SUSPENDED LOAD TIME SERIES

225 The available SSL time series range from 3 to 10 years (Table 1). For each catchment,  
226 the water discharges  $Q$  were calculated from automated measurements of the water  
227 levels with a frequency of 1 h. Stage-discharge rating curves were obtained thanks to  
228 numerous technics (Acoustic Doppler Current Profiler, salt-dilution, current meters or  
229 Large Scale Particle Image Velocimetry techniques), regularly performed during the  
230 study period. The surrogate technique for SSC estimation (i.e., turbidity-meter), coupled  
231 with direct sampling of SSC for calibration was used as commonly done for such field  
232 monitoring [*Mano et al.*, 2009; *Navratil et al.*, 2011]. SSC was assumed to be uniform  
233 over the cross section owing to the high levels of turbulence in these rivers, generating  
234 well-mixed flows. SSL was computed by multiplying SSC and  $Q$  at a 1-h frequency.

## 235 2.3. HYSTERESIS ANALYSIS TOOLS

236 In order to determine the dominant hysteresis pattern for the ten alpine catchments, a  
237 database of runoff events was created. Individual events were selected considering both  
238 SSL and SSC. In a first step, the events having a maximum SSL below a given  
239 threshold were not considered. A SSL threshold value ( $SSL_{1\%}$ ) was used, corresponding  
240 to the value below which 1% of the cumulated suspended sediment fluxes were  
241 transported (Figure 3). A similar approach was adopted to remove events exhibiting

242 SSC values below a threshold corresponding to 1% of the cumulated suspended  
243 sediment fluxes ( $SSC_{1\%}$ ).

244 **Figure 3**

245 The normalized index ( $HI_{Lloyd}$ ) proposed by Lloyd et al. (2016) was used (Eq. 3). This  
246 non-dimensional index is non-sensitive to the absolute value of SSC and Q, which  
247 makes it possible to do inter-event and inter-catchment comparison of hysteresis  
248 strength and direction. This index tends towards +1 for clockwise loops and towards -1  
249 for counterclockwise loops.

250 To compute  $HI_{Lloyd}$  for a given event, SSC and Q were normalized using their minimum  
251 and maximum values (Eq. 1 and Eq. 2) to obtain  $SSC^*$  and  $Q^*$ . The differences between  
252  $SSC^*$  monitored during the rising and the falling limb were then computed for each of the  
253 100 values of  $Q^*$  ranging between 0.01 and 1 (Figure 4). Finally,  $HI_{Lloyd}$  corresponds to  
254 the mean of these differences (Eq. 3).

255 **Figure 4**

$$SSC_i^* = \frac{SSC_i - SSC_{min}}{SSC_{max} - SSC_{min}} \quad (1)$$

$$Q_i^* = \frac{Q_i - Q_{min}}{Q_{max} - Q_{min}} \quad (2)$$

$$HI_{Lloyd} = mean \left[ SSC_i^*_{rising}(Q_i^*) - SSC_i^*_{falling}(Q_i^*) \right] \quad (3)$$

$$i \in [0.01,1]$$

256 For each catchment and each selected events, a  $HI_{Lloyd}$  value was calculated. The  
257 median value was considered representative of the dominant hysteresis patterns  
258 ( $median(HI_{Lloyd})$ ). However, the most frequent hysteresis patterns might not  
259 necessarily be those that transport most of the fine sediments. Thus, a new index ( $HI_{MS}$ )  
260 was introduced to investigate the “transport efficiency” associated to hysteresis. This  
261 was achieved by weighting each event by the transported mass ( $MS_i$ ):

$$HI_{MS} = \frac{\sum(HI_{Lloyd_i} \times MS_i)}{\sum MS_i} \quad (4)$$

262 Whereas several  $HI_{Lloyd}$  index are calculated (one for each event), only one  $HI_{MS}$  index is  
263 calculated (for the series of events) and inform which  $HI_{Lloyd}$  index is associated with the  
264 maximum transport.

265 These two continuous indexes were completed with classic pattern classifications  
266 [Gellis, 2013; Williams, 1989]. Hysteresis patterns were arbitrarily considered as  
267 clockwise when at least 80% of positive differences were observed between  $SSC^*$  during  
268 the rising and falling limb ( $Nb_{cl}$ ). Counterclockwise loops were considered when at least  
269 80% of negative differences were obtained ( $Nb_{ccl}$ ). Otherwise, the flood was considered  
270 to have a complex hysteresis patterns or no hysteresis ( $Nb_{complex}$ ). Finally, the  
271 percentages of the mass transported as clockwise hysteresis ( $MS_{cl}$ ), as  
272 counterclockwise hysteresis ( $MS_{ccl}$ ), and as complex or no hysteresis ( $MS_{complex}$ ) were  
273 calculated for each catchment. This classification permits a direct comparison between  
274 the number of events having a certain shape and the mass exported within this shape.

#### 275 2.4. SEDIMENT SOURCES CHARACTERIZATION

276 **Figure 5**

277 An analysis of each catchment was performed following the conceptual sediment  
278 sources description (river bed vs hillslopes) proposed by Bogen (1980) and often  
279 considered for qualitative hysteresis interpretations at the catchment scale [*Buendia et*  
280 *al.*, 2016; *Guillon et al.*, 2018; *Mao and Carrillo*, 2016; *Smith and Dragovich*, 2009].  
281 According to connectivity concepts developed by *Borselli et al.* (2008) and *Cavalli et al.*  
282 (2013), the area of eroded patches and the traveling distance needed to reach the outlet  
283 from these zones are important factors controlling the catchment connectivity. Also,  
284 according to numerous studies on fine sediments storage in the river network, the river  
285 width and the river bed area are parameters that have a strong control on the quantity of  
286 fine particles that can be stored in the river bed [*Collins and Walling*, 2007; *Lambert and*  
287 *Walling*, 1988; *Navratil et al.*, 2010; *Piqué et al.*, 2014]. These latter parameters may  
288 also be good proxies of the buffering capacity of the river bed and of its influence on fine  
289 sediments connectivity. Indeed, the exchanging surface between the flow and the river  
290 bed may have important control on fine particles infiltration in the gravel matrix [*Frostick*  
291 *et al.*, 1984; *Mooneyham and Strom*, 2018].

292 Following these evidences, a simplified sediment sources characterization was  
293 developed. The surface occupied by the active river channel width was considered as  
294 the first type of sediment source, whereas eroded areas were considered as the second  
295 type (Figure 5). The erosion maps described in section 2.1 were used for eroded areas  
296 identification. The distance needed by the water to reach the measuring station for each  
297 of these eroded area was estimated by using a digital elevation model with 25-m  
298 horizontal resolution and various algorithms of the Spatial Analyst toolbox of ARCGIS

299 10.3 (Fill, FlowLength, and FlowDirection). This water path from eroded areas to the  
300 outlet of the basin was calculated by considering the maximum slope for each grid of the  
301 digital elevation model. For a given location in the watershed, and considering the total  
302 area between this point and the measuring station downstream, we defined the  
303 cumulative eroded area as the sum of the eroded patches area ( $A_{eroded\ cum}$ ) and the  
304 cumulative area of the river bed as the sum of the active channel area ( $A_{bed\ cum}$ ), which  
305 was extracted using the active channel width digitalization. These two cumulative areas  
306 as well as their ratio ( $A_{eroded\ cum}/A_{bed\ cum}$ ) were calculated for each distance  $x$  from the  
307 monitoring station, with an incremental spatial step of 20 m, from downstream to  
308 upstream. For each catchment, the most upstream point was arbitrarily defined by a  
309 drainage area threshold of 1 km<sup>2</sup>. This point was located at a flow distance  $L$  from the  
310 outlet. Finally, the Sources Configuration Index ( $SCI_x$ ) was defined as the mean of the  
311 ratios ( $A_{eroded\ cum}/A_{bed\ cum}$ ) calculated for the first  $x$  percent of the distance  $L$ :

$$SCI_x = mean\left(\frac{A_{eroded\ cum}(i)}{A_{bed\ cum}(i)}\right), i \in [0; x] \quad (5)$$

312 This geomorphological index gives information on the relative importance of each type of  
313 sediment source depending on the distance from the measuring station. It is a simplified  
314 description developed to test the reliability of usual qualitative interpretation made for  
315 hysteresis patterns (hillslopes vs river bed). The slope is not explicitly taken into account  
316 even if it is often negatively correlated with the active river width. Likewise, local  
317 weighting factors (roughness or land use in Borselli *et al.* (2008) and Cavalli *et al.*  
318 (2013)) that could better describe the capacity to produce, transfer or store fine



319 sediments were not considered as they were difficult to estimate “a posteriori” and more  
320 questionable for suspended load than for bedload or debris flow processes.

321 This simple index permits to compare different spatial sources configuration (Figure 6).  
322 For instance, simplified conceptual cases (a) and (b) could probably lead to different  
323 hysteresis patterns at the outlet of the basin even if they have similar total cumulated  
324 bed and eroded area at the catchment scale. In case (a), eroded areas are located in  
325 the upper part of the basin whereas large storage zones of the river bed are located in  
326 the downstream part close to the monitoring station. Case (b) has the same bed  
327 configuration but eroded areas are located much closer to the outlet of the catchment  
328 ( $d_1 \gg d_2$ ). In that case, the ratio ( $A_{eroded\ cum}/A_{bed\ cum}$ ) increases much closer to the  
329 outlet than in case (a). Calculating the mean value of this ratio on a given distance  
330 permits to discriminate between these two cases. They have the same  $A_{eroded\ cum}/$   
331  $A_{bed\ cum}$  ratio considering the total length ( $x=100\%$ ), but the mean of these ratios  
332 calculated for  $x$  between 0% and 100% ( $SCI_{100}$ , average of the red curve in Figure 6) is  
333 much lower in case (a) than in case (b). Comparing conceptual cases (a) and (c)  
334 highlights the capacity of the index to compare different buffering effect played by the  
335 river bed. These cases have similar eroded areas located at the same distance from  
336 outlet ( $d_1$ ) but the cumulative bed area is much lower in case (c). Eroded areas could be  
337 less buffered in case (c) than in case (a). The mean value of the  $A_{eroded\ cum}/A_{bed\ cum}$   
338 ratio calculated for  $x$  between 0% and 100% ( $SCI_{100}$ ) will be smaller in case (a) than in  
339 case (c).

340 **Figure 6**

341 In order to discriminate the relative influence of hillslope sources and river bed on the  
342 hysteresis variability, an Eroded Area Index ( $EAI_x$ ) and a Bed Area Index ( $BAI_x$ ) were  
343 also defined and calculated for the ten catchments (Eq. 6 and Eq. 7).

$$EAI_x = \frac{\text{mean}(A_{eroded\ cum}(i))}{\max(A_{eroded\ cum})}, i \in [0; x] \quad (6)$$

$$BAI_x = \frac{\text{mean}(A_{bed\ cum}(i))}{\max(A_{bed\ cum})}, i \in [0; x] \quad (7)$$

## 344 3. RESULTS

### 345 3.1. RUNOFF EVENT CHARACTERISTICS

346 Following the event selection procedure (see Figure 3), the thresholds for SSL and SSC  
347 were calculated, and a dataset of events was created for each river (Table 2). More  
348 events were selected for northern catchments exhibiting daily floods during the melting  
349 season. While the observation periods were similar for the Glandon and the Asse, there  
350 were twice more selected events for the Glandon. Large differences were also observed  
351 in  $SSL_{1\%}$  and  $SSC_{1\%}$  values, e.g., the Galabre and the Bès rivers have suspended fluxes  
352 transported for higher values of SSC in comparison with other rivers.

353 **Table 2**

### 354 3.2. VARIABILITY OF DISCHARGE-CONCENTRATION HYSTERESIS IN ALPINE 355 CATCHMENTS

356 While the standard deviations of the  $HI_{Lloyd}$  were rather high for all catchments, some  
357 consistent observations can be made on the basis of the median  $HI_{Lloyd}$  (Table3, Figure  
358 7). Most rivers exhibited median values of  $HI_{Lloyd}$  around zero, because this value was  
359 often the most frequent and also because high positive or negative values had similar  
360 frequencies. This suggests an absence of a dominant hysteresis trend (clockwise or  
361 counterclockwise) in terms of the frequency of events having a certain shape. However,  
362 mainly clockwise loops ( $median(HI_{Lloyd}) >> 0$ ) were observed for the Buech, Drac, and  
363 Bléone catchments that have dominant braided bed morphology close to the monitoring  
364 stations, suggesting a more frequent contribution of the river bed sediment sources than  
365 in other catchments.

366 Different conclusions can be drawn when comparing the  $HI_{MS}$  index (most transporting)  
367 with the median (most frequent)  $HI_{Lloyd}$  index for each catchment (Table 3 and Figure 7).  
368 In northern catchments, median  $HI_{Lloyd}$  and  $HI_{MS}$  values were similar (maximum index  
369 difference of 0.02). However in the southern catchments, larger differences were  
370 observed between the two hysteresis indexes with differences ( $median(HI_{Lloyd})$  minus  
371  $HI_{MS}$ ) ranging between -0.13 and +0.16. Thus, the most frequent hysteresis shape was  
372 often not the most transport efficient one. For instance, 23% of events were classified as  
373 clockwise in the Asse and they contribute to 58% of the total SSL while 31% of events  
374 were classified as counterclockwise and contribute to only 11% of the total SSL. This  
375 suggests a higher transport efficiency of clockwise hysteresis patterns than  
376 counterclockwise ones.

377 **Table 3**

378 **Figure 7**

### 379 3.3. SEDIMENT SOURCES ANALYSIS

380 Large differences in the relative location of river bed and eroded area sediment sources  
381 were observed between catchments. As shown in Figure 8b, the Arvan exhibited large  
382 eroded areas close to the measuring station with a limited bed area leading to a ratio of  
383  $A_{eroded\ cum}/A_{bed\ cum}$  equal to one at a distance of roughly 7 km. By contrast, for the  
384 Bléone, the bed area is larger than the eroded areas in the first 50 km close to the  
385 monitoring station (Figure 8-a). The cumulative eroded areas exceeded the cumulative  
386 bed areas only after 55 km.

387 **Figure 8**

388 To quantitatively compare these differences between the ten basins we plot in Figure 9:

- 389 -  $\frac{A_{eroded\ cum}(x)}{\max(A_{eroded\ cum})}$ : the fraction of the total cumulative eroded area as a function of the  
390 distance from the outlet,
- 391 -  $\frac{A_{bed\ cum}(x)}{\max(A_{bed\ cum})}$ : the fraction of the total cumulative bed area as a function of the  
392 distance from the outlet,
- 393 -  $SCI_x$ : the average values of the ratios  $A_{eroded\ cum}/A_{bed\ cum}$  calculated on a given  
394 distance upstream the outlet (0% to x%).

395 For the ten catchments, the cumulative bed area exhibited a relative constant increase  
396 with increasing distance to the outlet (Figure 9-a). This suggests that bed areas were, as  
397 a first approximation, homogeneously distributed along the x distance. In comparison,

398 the cumulative eroded area showed a more sudden increase with the increasing  
399 distance to the outlet (Figure 9-b). A small fraction of eroded area was located close to  
400 the monitoring stations as less than 50% of eroded areas are located for x distance  
401 smaller than 0.5 and less than 10% for x smaller than 0.2. Also, much more variability  
402 between the ten catchments was observed. For instance, the normalized cumulative  
403 eroded area of the Romanche basin starts to increase significantly for x around 0.5 while  
404 the Bléone basin showed a sudden increase for x larger than 0.8. This suggests that  
405 eroded areas were located more in the upstream part of the Bléone watershed than for  
406 the Romanche. Some catchments as the Arc basin exhibited a more smooth increase  
407 indicating a more homogeneous eroded patches distribution along the x distance.

408 Finally, the source configuration index  $SCI_x$  (Eq.5) shows for all rivers an increase in the  
409 relative importance of eroded areas as compared with bed areas when moving in the  
410 upstream direction (Figure 9-c). This confirms that river bed sources were closer to the  
411 measuring station than eroded areas sources. However, some small eroded tributaries  
412 could locally generate a high value of  $SCI_x$  near the observation station, as was the  
413 case for the Galabre River.  $SCI_x$  were highly variable from one catchment to another.  
414 The shortest distance considered ( $x=10\%$ ) to compute this index led to small  
415 differences between catchments whereas longer distances led to large differences. For  
416 instance, the two extreme cases, the Bléone and Arvan rivers, had the same  $SCI_{10}$  (0.1)  
417 but their  $SCI_{100}$  values were very different (0.3 and 21.3, respectively). The sources  
418 indexes ( $SCI_x$ ,  $BAI_x$ ,  $EAI_x$ ) values calculated for x ranging from 10% to 100% with a x  
419 step of 10% are provided as supplementary material for more details.

420 **Figure 9**

421 3.4. RELATION BETWEEN SEDIMENT SOURCES CONFIGURATION AND

422 DOMINANT HYSTERESIS PATTERNS

423 The general catchment characteristics, the index describing the river bed area  
424 distribution ( $BAI_x$ ), the index describing the eroded area distribution ( $EAI_x$ ) and the  
425 index comparing river bed and eroded area distribution ( $SCI_x$ ) were compared with the  
426 dominant hysteresis pattern for each catchment (Table 4). While some significant  
427 correlations were found between general catchment characteristics and hysteresis  
428 indexes, the values remained rather low and did not exceed 0.63. Overall the Lloyd  
429 hysteresis index ( $HI_{Lloyd}$ ) exhibited only limited and small significant correlations with the  
430 three sediment sources indexes ( $SCI_x$ ,  $BAI_x$ ,  $EAI_x$ ), in comparison with the mass  
431 weighted hysteresis index ( $HI_{MS}$ ).

432 Significant negative correlations ( $\rho < -0.98$ ,  $pvalue < 0.01$ ) were found between  $HI_{MS}$   
433 and the sediment sources index ( $SCI_x$ , Figure 10 and Table 4). This result suggests that  
434 the part of the fluxes exported with clockwise loops decreases when the relative  
435 importance of the eroded areas relative to the bed areas increases. Lower but also  
436 significant negative correlations ( $\rho < -0.71$ ,  $pvalue < 0.01$ ) were obtained between the  
437 mass weighted hysteresis index ( $HI_{MS}$ ) and the eroded area distribution index ( $EAI_x$ )  
438 while no significant correlations were obtained between  $HI_{MS}$  and the bed area  
439 distribution index ( $BAI_x$ ). It indicates that the spatial distribution of eroded areas in the  
440 catchment is an important factor for explaining the hysteresis variability while river bed  
441 area distribution alone cannot explain this variability. However using both information  
442 (i.e. bed area distribution combined with eroded area distribution,  $SCI_x$ ) permits a much

443 better explanation of the hysteresis variability between catchments than considering  
444 eroded area distribution alone.

445 The correlation between the mass weighted hysteresis index  $HI_{MS}$  and the sediment  
446 source configuration index  $SCI_x$  (in a lesser extent with eroded area distribution index  
447  $EAI_x$ ) was found to increase when averaging the values over increasing distance ( $x$ )  
448 from the outlet. Both explanatory variables reached their maximum correlation value at a  
449 distance upstream of the monitoring station of approximately 70% (Table 4 and Figure  
450 10). The closest source configuration indexes were not found to explain the variability of  
451 hysteresis patterns between catchments, suggesting that close source configurations  
452 alone cannot explain the suspended load dynamics.

453 **Table 4**

454 **Figure 10**

## 455 4. DISCUSSION

### 456 4.1. DOMINANT HYSTERESIS PATTERNS AND TRANSPORT EFFICIENCY

457 Hysteresis effects are usually analyzed by counting the number of events having a  
458 certain shape [Aguilera and Melack, 2018; Aich et al., 2014; Buendia et al., 2016;  
459 Hamshaw et al., 2018; Navratil et al., 2010]. However, the comparison done in this study  
460 of ten contrasted alpine catchments highlighted that different results can be obtained by  
461 considering the fluxes transported with a given shape (Figure 7). From these results, two  
462 recommendations can be made, depending on the objective of the study. For those

463 aiming at identifying the dominant sediment production processes for a given catchment,  
464 the hysteresis analysis should necessarily consider the intensity of each event, i.e., the  
465 average mass weighted hysteresis index. For studies aiming at understanding more in  
466 detail the hydro-sedimentary catchment functioning both in terms of occurrence and  
467 efficiency of the events transporting fine sediments, the analysis of hysteresis should be  
468 done simultaneously for both indexes. In our case, no relation was found between the  
469 median value of the Lloyd hysteresis index ( $HI_{Lloyd}$ ) considering the number of events  
470 and any sediment source index ( $SCI_x$ ,  $EAI_x$ ,  $BAI_x$ ) while significant correlations were  
471 found with the average mass weighted index. This suggests that the transport efficiency  
472 of hysteresis loops should be considered as a proxy of sediment production processes.

473 Calculating the two indices also allowed us to observe distinct behaviors for the ten  
474 alpine catchments. The differences between the fluxes exported and the frequency of  
475 events having a certain hysteresis shape were much higher for the southern catchments  
476 including the Buëch River than for the northern ones (Figure 7). This could be due to  
477 differences in hydrological regimes (Figure 2). Indeed, the southern catchments  
478 exhibited a more pronounced seasonal variability of the hysteresis values than the  
479 northern ones (Figure 11). Counterclockwise patterns were mainly observed during  
480 summer, corresponding to dry periods associated to short and intense convective  
481 storms. Clockwise patterns were observed during wet periods characterized by low  
482 intensity but rather long precipitation events leading to larger rainfall amounts than  
483 during summer. These results were consistent with those from Navratil et al. (2012)  
484 reporting that clockwise hysteresis loops exported the bulk of total suspended load  
485 during widespread flood events in the Bléone catchment. They observed marked



486 counterclockwise loops during summer rainstorms in upper tributaries which generate  
487 suspended fluxes that were not efficiently transferred downstream. This might explain  
488 why large differences were observed between the frequency and the fluxes exported  
489 with a given hysteresis for these southern basins. Similar trends were observed by Soler  
490 *et al.* (2008) or Buendia *et al.* (2016) in Pyrenean catchments having similar hydrological  
491 regimes. In comparison, the northern catchments exhibited a much more constant  
492 export of fine sediments during the frequent daily flood events of the melting season.  
493 Many more flood events were observed for similar monitoring periods in the north than in  
494 the south (Table 2). Mano *et al.* (2009) reported that 90% of the suspended fluxes were  
495 transported in 5% and 7% of the time for the Bléone and Asse Rivers, respectively, while  
496 25% of the time was needed for the Romanche River.

497 **Figure 11**

#### 498 4.2. INFLUENCE OF CATCHMENT GEOMORPHOLOGICAL CHARACTERISTICS

499 The relation between the mass weighted hysteresis and catchment sources  
500 configuration (river bed vs. eroded areas) is consistent with previous findings and typical  
501 qualitative analyses of the hysteresis patterns which considers that a counterclockwise  
502 loops indicates a distant contribution while a clockwise loop results from a relatively  
503 close source mobilization [*Bogen, 1980; Gellis, 2013; Guillon et al., 2018; Mao and*  
504 *Carrillo, 2016; Navratil et al., 2012; Navratil et al., 2010; Smith and Dragovich, 2009*].  
505 Influence of watershed characteristics on SSL hysteresis patterns was observed by  
506 Aguilera *et al.* (2018) in ten mountainous Californian catchments. Also, using a random  
507 forest model on 45 measuring stations, Vaughan *et al.* (2017) showed that considering

508 near-channel morphological characteristics in addition to land use contributes to a better  
509 explanation of the sediment rating curve parameters than using land use only. Their  
510 random forest model explained 38% and 43% of the hysteresis variance when  
511 considering respectively only watershed metrics or watershed plus near channel metrics.  
512 In our analysis, we also observed that both sources need to be considered. However our  
513 results show the importance to consider not only global catchments properties but the  
514 relative importance of these two types of sources (bed vs eroded areas) as well as their  
515 “travelling distance” to the monitoring station to explain hysteresis variability between  
516 catchments. Also, as was observed by Vaughan et al. (2017), we should stress that  
517 including the bed area information by considering the relative spatial distribution of  
518 eroded versus bed area ( $SCI_x$ ) and not the spatial distribution of eroded area ( $EAI_x$ )  
519 alone, permits a much better explanation of the hysteresis variability and thus of the  
520 suspended load dynamics. This result is also consistent with several studies that  
521 reported a significant buffering effect played by the river bed which could be considered  
522 as a significant fine sediment source in mountainous catchments having relatively large  
523 and active alluvial reaches [Guillon et al., 2018; Navratil et al., 2012; Navratil et al.,  
524 2010; Orwin and Smart, 2004].

525 The results obtained in this paper and in previous studies bring us to propose the  
526 following conceptual description of hysteresis and sediment configuration interactions  
527 (Figure 12). The dominant hysteresis effect observed at a given location in a catchment  
528 could depend on the upstream capacity to produce distant erosion and to buffer these  
529 upstream fluxes. If the remobilization of fine sediments from the river bed did not exist,  
530 mainly counterclockwise hysteresis should have been observed because of celerity

531 differences between the flow rate and SSC waves [*Klein*, 1984]. Thus, the hysteresis  
532 patterns would depend on the location of the observation point for a given  
533 geomorphological scale (point A, B, C or D in Figure 12). Following the conceptual  
534 configuration in Figure 12, the fraction of SSL coming from the river bed and driven by  
535 the total flow rate could increase when moving to the downstream part of a catchment,  
536 while SSL coming directly from primary hillslope sources and driven by rainfall or runoff  
537 could decrease. Such scale dependencies of hysteresis processes have been already  
538 noticed in hydrological studies [*Gharari and Razavi*, 2018]. For instance, *Davies and*  
539 *Beven* (2015) have shown by using a synthetic case that hysteresis between streamflow  
540 and catchment storage was changing with the catchment size considered.

541 **Figure 12**

#### 542 4.3. LIMITATIONS AND IMPLICATIONS

543 Given the wide range of characteristics of the 10 studied alpine catchments, comprising  
544 various sizes, geologies, altitudes, hydrological and sedimentary regimes the proposed  
545 approach can be considered as relevant in other mountainous environments. However,  
546 its relevance should be tested in other contexts such as low-land, agricultural or arid  
547 environments. The analysis of the sediment sources might be improved to get a more  
548 detailed description of the catchment sources configuration to investigate its relation with  
549 suspended load at shorter spatial and temporal scales. For instance, the mechanical  
550 properties of rocks in eroded areas could be taken into account to give more importance  
551 to soft rocks than to more resistant ones for catchments with contrasted lithologies. The  
552 local river bed slope could also be explicitly considered in addition to the active river

553 width to get a proxy of the buffering capacity of the bed. This would probably give less  
554 importance to steep streams and more importance to gentle ones. These potential  
555 improvements might be tested in future work.

556 However, while the approach used does not represent all the complexity of interactions  
557 between suspended load and sediment source configuration a significant part of the  
558 variability of SSL hysteresis can be explained by this simplified source description at a  
559 regional scale. This confirms the strong link between hysteresis processes and the  
560 variable sediment sources activation that have been qualitatively described for decades  
561 [Gellis, 2013; Gharari and Razavi, 2018; Williams, 1989]. Our results suggest that even  
562 for small catchments, fine sediment dynamics and hysteresis effects could be largely  
563 influenced by erosion and deposition processes occurring in the river bed. This might be  
564 the case in catchments where eroded areas are located far enough upstream so that the  
565 main channel can act as a buffering reservoir of fine sediments. However, larger  
566 catchments with well-developed fluvial systems could, conversely, be influenced in a  
567 non-negligible way by hillslope process production if some eroded areas are located at a  
568 short distance from the monitoring station. Both processes are probably inevitably  
569 linked. The fractions of SSL coming from the bed or from the hillslopes seem to change  
570 depending on the point considered in the catchment. The simple sediment sources  
571 analysis proposed in this study could be performed prior to the installation of a gauging  
572 station or prior to modeling effort in order to assess which kind of processes should be  
573 considered in a conceptual modeling approach. It could also be helpful to determine the  
574 dominant fine sediment production process for river or dam management at the  
575 catchment scale.

## 576 5. CONCLUSIONS

577 This study aimed at testing the links between Discharge-Suspended Sediment  
578 Concentrations (Q-SSC) hysteresis and the spatial configuration of sediment sources  
579 which have been qualitatively considered for decades without been quantitatively tested.  
580 A quantitative analysis of sediment sources configuration and Q-SSC hysteresis was  
581 performed in ten contrasted alpine catchments. Hysteresis indexes were calculated on a  
582 high number of automated sampled events to extract the dominant hysteresis pattern for  
583 each catchment. Simple indexes were developed to describe the river bed and eroded  
584 patches area distribution as well as a “travelling distance to the outlet”. The main  
585 findings can be summarized as follows:

586 (i) Considering the dominant SSL hysteresis in a given catchment as the most  
587 frequent pattern or as the most efficient in terms of transport can lead to  
588 different results. Our observations suggest that the transport efficiency of  
589 hysteresis should be considered to infer the dominant sediment production  
590 process. This could be particularly true for catchments having most of their  
591 fluxes exported during few short events and exhibiting marked seasonal  
592 hysteresis variability. Thus an averaged mass weighted hysteresis index was  
593 proposed.

594 (ii) A strong correlation was found between mass weighted hysteresis index and  
595 sediment sources configuration index (river bed vs eroded area) which  
596 confirms the qualitative interpretations often made for SSC-Q hysteresis  
597 processes. We also observed that the sources configuration should be  
598 considered on a long enough fraction of the catchment (at least 50% of the

599 whole principal river network) upstream the observation point to explain the  
600 spatial hysteresis variability. This is consistent with the rather long travelled  
601 distances of suspended particles.

602 (iii) In comparison to previous studies, these results show the importance to  
603 consider not only general catchment properties or sediment sources to  
604 understand SSL dynamics but their spatial distribution and connectivity.  
605 Furthermore, including bed related information increases significantly the  
606 explanatory power of the SSC-Q hysteresis variability than using only primary  
607 hillslope sources information.

## 608 6. NOTATIONS

609 The following symbols are used in this paper.

<i>SSL</i>	Suspended sediment load
<i>SSC</i>	Suspended sediment concentration
<i>Q</i>	Flow rate
<i>A</i>	Catchment area
<i>No</i>	Fraction of catchment with low or no vegetation cover
<i>Fo</i>	Fraction of catchment forest cover
<i>Gl</i>	Fraction of catchment with glacier cover
<i>SCR</i>	Fraction of catchment with soft coherent rock cover
<i>HR</i>	Fraction of catchment with heterogeneous rock cover
<i>RR</i>	Fraction of catchment with resistant rock cover

$W_{10}$	Median active width extracted on the first 10 km upstream the station
$S_{10}$	Mean riverbed slope extracted on the first 10 km upstream the station
$q$	Mean annual specific discharge
$HI_{Lloyd}$	Lloyd hysteresis index
$SSC^*$	Normalized suspended sediment concentration at the flood scale
$Q^*$	Normalized flow rate at the flood scale
$HI_{Ms}$	Mass weighted average hysteresis index
$MS_i$	Mass of suspended sediment transported during the event i
$Nb_{cl}$	Fraction of event having a clockwise hysteresis shape
$Nb_{ccl}$	Fraction of event having a counterclockwise hysteresis shape
$Nb_{complex}$	Fraction of event having complex or no hysteresis shape
$MS_{cl}$	Fraction of the mass exported with a clockwise hysteresis shape
$MS_{ccl}$	Fraction of the mass exported with a counterclockwise hysteresis shape
$MS_{complex}$	Fraction of the mass exported with complex or no hysteresis hysteresis
$A_{eroded\ cum}$	Cumulative eroded area at a given distance from the station
$A_{bed\ cum}$	Cumulative riverbed area at a given distance from the station
$SCI_x$	Sources Configuration Index (mean ratio of cumulative eroded area over cumulative bed area calculated on the first x% of the main channel length)
$EAI_x$	Eroded Area Index (mean cumulative eroded area over total eroded area on the first x% of the main channel length)
$BAI_x$	Bed Area Index (mean cumulative bed area over total bed area on the first x% of the main channel length)
$L$	Maximum distance used to compute the sediment source configuration

	index
$SSL_{99\%}$	Threshold on SSL above which 99% of cumulated suspended fluxes are transported
$SSC_{99\%}$	Threshold on SSC above which 99% of cumulated suspended fluxes are transported
$t_{exceed}$	Minimum time step for which a SSL should exceed all following and preceding values for the event detection

## 610 7. ACKNOWLEDGEMENTS

611 This study was founded by IRSTEA (National Research Institute of Science and  
612 Technology for the Environment and Agriculture) and EDF (Electricité de France). The  
613 field monitoring data provided by IRSTEA, EDF and IGE (Institute for Geosciences and  
614 Environmental research) field teams are greatly appreciated. The authors also want to  
615 thank three anonymous reviewers who greatly contributed to improve to this paper by  
616 providing helpful reviews of an earlier version of this manuscript.

## 617 8. REFERENCES

- 618 Aguilera, R., and J. M. Melack (2018), Concentration-Discharge Responses to Storm  
619 Events in Coastal California Watersheds, *Water Resources Research*, 54(1), 407-424,  
620 doi:10.1002/2017wr021578.
- 621 Aich, V., A. Zimmermann, and H. Elsenbeer (2014), Quantification and interpretation of  
622 suspended-sediment discharge hysteresis patterns: How much data do we need?,  
623 *Catena*, 122, 120-129, doi:10.1016/j.catena.2014.06.020.



- 624 Andermann, C., A. Crave, R. Gloaguen, P. Davy, and S. Bonnet (2012), Connecting  
625 source and transport: Suspended sediments in the Nepal Himalayas, *Earth and*  
626 *Planetary Science Letters*, 351-352, 158-170, doi:10.1016/j.epsl.2012.06.059.
- 627 Asselman, N. E. M. (1999), Suspended sediment dynamics in a large drainage basin:  
628 the River Rhine, *hydrological Processes*, 13, 1437-1450, doi:10.1002/(SICI)1099-  
629 1085(199907)13:10<1437::AID-HYP821>3.0.CO;2-J.
- 630 Baca, P. (2010), Hysteresis effect in suspended sediment concentration in the Rybárik  
631 basin, Slovakia / Effet d'hystérèse dans la concentration des sédiments en suspension  
632 dans le bassin versant de Rybárik (Slovaquie), *Hydrological Sciences Journal*, 53(1),  
633 224-235, doi:10.1623/hysj.53.1.224.
- 634 Bertrand, M. (2014), PhD thesis : Debris-flow susceptibility assessment at the regional  
635 scale of the Southern French Alps, Ecole normale supérieure de lyon, <NNT :  
636 2014ENSL0895>. <tel-01022867>.
- 637 Bertrand, M., F. Liébault, and H. Piégay (2017), Regional Scale Mapping of Debris-Flow  
638 Susceptibility in the Southern French Alps, *Revue de géographie alpine*(105-4),  
639 doi:10.4000/rga.3543.
- 640 Bogen, J. (1980), The hysteresis effect of sediment transport systems, *Norsk Geografisk*  
641 *Tidsskrift - Norwegian Journal of Geography*, 34(1), 45-54,  
642 doi:10.1080/00291958008545338.
- 643 Borselli, L., P. Cassi, and D. Torri (2008), Prolegomena to sediment and flow  
644 connectivity in the landscape: A GIS and field numerical assessment, *Catena*, 75(3),  
645 268-277, doi:10.1016/j.catena.2008.07.006.
- 646 Buendia, C., D. Vericat, R. J. Batalla, and C. N. Gibbins (2016), Temporal Dynamics of  
647 Sediment Transport and Transient In-channel Storage in a Highly Erodible Catchment,  
648 *Land Degradation & Development*, 27(4), 1045-1063, doi:10.1002/ldr.2348.
- 649 Cavalli, M., S. Trevisani, F. Comiti, and L. Marchi (2013), Geomorphometric assessment  
650 of spatial sediment connectivity in small Alpine catchments, *Geomorphology*, 188, 31-  
651 41, doi:10.1016/j.geomorph.2012.05.007.
- 652 Collins, A. L., and D. E. Walling (2007), The storage and provenance of fine sediment on  
653 the channel bed of two contrasting lowland permeable catchments, UK, *River Research*  
654 *and Applications*, 23(4), 429-450, doi:10.1002/rra.992.
- 655 Davies, J. A. C., and K. Beven (2015), Hysteresis and scale in catchment storage, flow  
656 and transport, *Hydrological Processes*, 29(16), 3604-3615, doi:10.1002/hyp.10511.

- 657 de Vente, J., J. Poesen, P. Bazzoffi, A. V. Rompaey, and G. Verstraeten (2006),  
658 Predicting catchment sediment yield in Mediterranean environments: the importance of  
659 sediment sources and connectivity in Italian drainage basins, *Earth Surface Processes  
660 and Landforms*, 31(8), 1017-1034, doi:10.1002/esp.1305.
- 661 Douglas, I. A. N. (1967), Man, Vegetation and the Sediment Yields of Rivers, *Nature*,  
662 215(5104), 925-928, doi:10.1038/215925a0.
- 663 Duvert, C., N. Gratiot, O. Evrard, O. Navratil, J. Nemery, C. Prat, and M. Esteves (2010),  
664 Drivers of erosion and suspended sediment transport in three headwater catchments of  
665 the Mexican Central Highlands, *Geomorphology*, 123(3-4), 243-256,  
666 doi:10.1016/j.geomorph.2010.07.016.
- 667 Duvert, C., et al. (2012), Towards prediction of suspended sediment yield from peak  
668 discharge in small erodible mountainous catchments (0.45–22km<sup>2</sup>) of France, Mexico  
669 and Spain, *Journal of Hydrology*, 454-455, 42-55, doi:10.1016/j.jhydrol.2012.05.048.
- 670 Esteves, M., C. Legout, O. Navratil, and O. Evrard (2018), Medium term high frequency  
671 observation of discharge and suspended sediment in a Mediterranean mountainous  
672 catchment, *Journal of Hydrology*, *Accepted*.
- 673 Frostick, L. E., P. M. Lucas, and I. Reid (1984), The infiltration of fine matrices into  
674 coarse-grained alluvial sediments and its implications for stratigraphical interpretation  
675 *Journal of the Geological Society*, 141(6), 955-965, doi:10.1144/gsjgs.141.6.0955.
- 676 Gellis, A. C. (2013), Factors influencing storm-generated suspended-sediment  
677 concentrations and loads in four basins of contrasting land use, humid-tropical Puerto  
678 Rico, *Catena*, 104, 39-57, doi:10.1016/j.catena.2012.10.018.
- 679 Gharari, S., and S. Razavi (2018), A review and synthesis of hysteresis in hydrology and  
680 hydrological modeling: Memory, path-dependency, or missing physics?, *Journal of  
681 Hydrology*, 566, 500-519, doi:10.1016/j.jhydrol.2018.06.037.
- 682 Guillon, H., J.-L. Mugnier, and J.-F. Buoncristiani (2018), Proglacial sediment dynamics  
683 from daily to seasonal scales in a glaciated Alpine catchment (Bossons glacier, Mont  
684 Blanc massif, France), *Earth Surface Processes and Landforms*, 43(7), 1478-1495,  
685 doi:10.1002/esp.4333.
- 686 Haas, F., T. Heckmann, V. Wichmann, and M. Becht (2011), Quantification and  
687 Modeling of Fluvial Bedload Discharge from Hillslope Channels in two Alpine  
688 Catchments (Bavarian Alps, Germany), *Zeitschrift für Geomorphologie, Supplementary  
689 Issues*, 55(3), 147-168, doi:10.1127/0372-8854/2011/0055s3-0056.

- 690 Hamshaw, S. D., M. M. Dewoolkar, A. W. Schroth, B. C. Wemple, and D. M. Rizzo  
691 (2018), A New Machine-Learning Approach for Classifying Hysteresis in Suspended-  
692 Sediment Discharge Relationships Using High-Frequency Monitoring Data, *Water*  
693 *Resources Research*, 54(6), 4040-4058, doi:10.1029/2017wr022238.
- 694 Heckmann, T., M. Cavalli, O. Cerdan, S. Foerster, M. Javaux, E. Lode, A. Smetanová,  
695 D. Vericat, and F. Brardinoni (2018), Indices of sediment connectivity: opportunities,  
696 challenges and limitations, *Earth-Science Reviews*, 187, 77-108,  
697 doi:10.1016/j.earscirev.2018.08.004.
- 698 Heckmann, T., and W. Schwanghart (2013), Geomorphic coupling and sediment  
699 connectivity in an alpine catchment — Exploring sediment cascades using graph theory,  
700 *Geomorphology*, 182, 89-103, doi:10.1016/j.geomorph.2012.10.033.
- 701 Jansson, M. B. (2002), Determining sediment source areas in a tropical river basin,  
702 Costa Rica, *Catena*, 47, 63–84, doi:0341-8162/02/\$.
- 703 Klein, M. (1984), Anti clockwise hysteresis in suspended sediment concentration during  
704 individual storms: Holbeck Catchment; Yorkshire, England, *Catena*, 11, 251-257,  
705 doi:https://doi.org/10.1016/0341-8162(84)90014-6.
- 706 Lambert, C. P., and D. E. Walling (1988), Measurement of Channel Storage of  
707 Suspended Sediment in a Gravel-Bed River, *Catena*, 15(1), 65-80, doi:10.1016/0341-  
708 8162(88)90017-3.
- 709 Landers, M. N., and T. W. Sturm (2013), Hysteresis in suspended sediment to turbidity  
710 relations due to changing particle size distributions, *Water Resources Research*, 49(9),  
711 5487-5500, doi:10.1002/wrcr.20394.
- 712 Le Pape, O., et al. (2013), Sources of organic matter for flatfish juveniles in coastal and  
713 estuarine nursery grounds: A meta-analysis for the common sole (*Solea solea*) in  
714 contrasted systems of Western Europe, *Journal of Sea Research*, 75, 85-95,  
715 doi:10.1016/j.seares.2012.05.003.
- 716 Lefrançois, J., C. Grimaldi, C. Gascuel-Oudou, and N. Gilliet (2007), Suspended  
717 sediment and discharge relationships to identify bank degradation as a main sediment  
718 source on small agricultural catchments, *Hydrological Processes*, 21(21), 2923-2933,  
719 doi:10.1002/hyp.6509.
- 720 Legout, C., J. Poulénard, J. Nemery, O. Navratil, T. Grangeon, O. Evrard, and M.  
721 Esteves (2013), Quantifying suspended sediment sources during runoff events in  
722 headwater catchments using spectroradiometry, *Journal of Soils and Sediments*, 13(8),  
723 1478-1492, doi:10.1007/s11368-013-0728-9.

- 724 Lloyd, C. E., J. E. Freer, P. J. Johnes, and A. L. Collins (2016), Using hysteresis  
725 analysis of high-resolution water quality monitoring data, including uncertainty, to infer  
726 controls on nutrient and sediment transfer in catchments, *Sci Total Environ*, 543(Pt A),  
727 388-404, doi:10.1016/j.scitotenv.2015.11.028.
- 728 Ludwig, W., and J. L. Probst (1998), River sediment discharge to the oceans; present-  
729 day controls and global budgets, *American Journal of Science*, 298(4), 265-295,  
730 doi:10.2475/ajs.298.4.265.
- 731 Mano, V., J. Nemery, P. Belleudy, and A. Poirel (2009), Assessment of suspended  
732 sediment transport in four alpine watersheds (France): influence of the climatic regime,  
733 *Hydrological Processes*, 23(5), 777-792, doi:10.1002/hyp.7178.
- 734 Mao, L., and R. Carrillo (2016), Temporal dynamics of suspended sediment transport in  
735 a glacierized Andean basin, *Geomorphology*, doi:10.1016/j.geomorph.2016.02.003.
- 736 Marden, M., G. Arnold, B. Gomez, and D. Rowan (2005), Pre- and post-reforestation  
737 gully development in Mangatu Forest, East Coast, North Island, New Zealand, *River*  
738 *Research and Applications*, 21(7), 757-771, doi:10.1002/rra.882.
- 739 Marttila, H., and B. Kløve (2010), Dynamics of erosion and suspended sediment  
740 transport from drained peatland forestry, *Journal of Hydrology*, 388(3-4), 414-425,  
741 doi:10.1016/j.jhydrol.2010.05.026.
- 742 Meybeck, M., L. Laroche, H. H. Dürr, and J. P. M. Syvitski (2003), Global variability of  
743 daily total suspended solids and their fluxes in rivers, *Global and Planetary Change*,  
744 39(1-2), 65-93, doi:10.1016/s0921-8181(03)00018-3.
- 745 Mooneyham, C., and K. Strom (2018), Deposition of Suspended Clay to Open and  
746 Sand-Filled Framework Gravel Beds in a Laboratory Flume, *Water Resources*  
747 *Research*, doi:10.1002/2017wr020748.
- 748 Navratil, O., M. Esteves, C. Legout, N. Gratiot, J. Nemery, S. Willmore, and T. Grangeon  
749 (2011), Global uncertainty analysis of suspended sediment monitoring using turbidimeter  
750 in a small mountainous river catchment, *Journal of Hydrology*, 398(3-4), 246-259,  
751 doi:10.1016/j.jhydrol.2010.12.025.
- 752 Navratil, O., et al. (2012), Temporal variability of suspended sediment sources in an  
753 alpine catchment combining river/rainfall monitoring and sediment fingerprinting, *Earth*  
754 *Surface Processes and Landforms*, 37(8), 828-846, doi:10.1002/esp.3201.
- 755 Navratil, O., C. Legout, D. Gateuille, M. Esteves, and F. Liebault (2010), Assessment of  
756 intermediate fine sediment storage in a braided river reach (southern French Prealps),  
757 *Hydrological Processes*, 24(10), 1318-1332, doi:10.1002/hyp.7594.

- 758 Nistor, C. J., and M. Church (2005), Suspended sediment transport regime in a debris-  
759 flow gully on Vancouver Island, British Columbia, *Hydrological Processes*, 19(4), 861-  
760 885, doi:10.1002/hyp.5549.
- 761 Orwin, J. F., and C. C. Smart (2004), Short-term spatial and temporal patterns of  
762 suspended sediment transfer in proglacial channels, Small River Glacier, Canada,  
763 *Hydrological Processes*, 18(9), 1521-1542, doi:10.1002/hyp.1402.
- 764 Park, J., and J. R. Hunt (2017), Coupling fine particle and bedload transport in gravel-  
765 bedded streams, *Journal of Hydrology*, 552, 532-543, doi:10.1016/j.jhydrol.2017.07.023.
- 766 Parsons, A. J., L. Bracken, R. E. Poepl, J. Wainwright, and S. D. Keesstra (2015),  
767 Introduction to special issue on connectivity in water and sediment dynamics, *Earth*  
768 *Surface Processes and Landforms*, 40(9), 1275-1277, doi:10.1002/esp.3714.
- 769 Picouet, C., B. Hingray, and J. C. Olivry (2009), Modelling the suspended sediment  
770 dynamics of a large tropical river: the Upper Niger river basin at Banankoro, *Hydrological*  
771 *Processes*, 23(22), 3193-3200, doi:10.1002/hyp.7398.
- 772 Piqué, G., J. A. López-Tarazón, and R. J. Batalla (2014), Variability of in-channel  
773 sediment storage in a river draining highly erodible areas (the Isábena, Ebro Basin),  
774 *Journal of Soils and Sediments*, 14(12), 2031-2044, doi:10.1007/s11368-014-0957-6.
- 775 Roux, C., A. Alber, M. Bertrand, L. Vaudor, and H. Piégay (2015), "FluvialCorridor": A  
776 new ArcGIS toolbox package for multiscale riverscape exploration, *Geomorphology*,  
777 242, 29-37, doi:10.1016/j.geomorph.2014.04.018.
- 778 Smith, H. G., and D. Dragovich (2009), Interpreting sediment delivery processes using  
779 suspended sediment-discharge hysteresis patterns from nested upland catchments,  
780 south-eastern Australia, *Hydrological Processes*, 23(17), 2415-2426,  
781 doi:10.1002/hyp.7357.
- 782 Soler, M., J. Latron, and F. Gallart (2008), Relationships between suspended sediment  
783 concentrations and discharge in two small research basins in a mountainous  
784 Mediterranean area (Vallcebre, Eastern Pyrenees), *Geomorphology*, 98(1-2), 143-152,  
785 doi:10.1016/j.geomorph.2007.02.032.
- 786 Sun, L., M. Yan, Q. Cai, and H. Fang (2016), Suspended sediment dynamics at different  
787 time scales in the Loushui River, south-central China, *Catena*, 136, 152-161,  
788 doi:10.1016/j.catena.2015.02.014.
- 789 Tananaev, N. I. (2012), Hysteresis effect in the seasonal variations in the relationship  
790 between water discharge and suspended load in rivers of permafrost zone in Siberia and  
791 Far East, *Water Resources*, 39(6), 648-656, doi:10.1134/s0097807812060073.

792 Tananaev, N. I. (2015), Hysteresis effects of suspended sediment transport in relation to  
793 geomorphic conditions and dominant sediment sources in medium and large rivers of  
794 the Russian Arctic, *Hydrology Research*, 46(2), doi:10.2166/nh.2013.199.

795 Trustrum, N. A., and P. R. Stephens (1981), Selection of hill-country pasture  
796 measurement sites by interpretation of sequential aerial photographs, *New Zealand*  
797 *Journal of Experimental Agriculture*, 9(1), 31-34, doi:10.1080/03015521.1981.10427799.

798 Vaughan, A. A., P. Belmont, C. P. Hawkins, and P. Wilcock (2017), Near-Channel  
799 Versus Watershed Controls on Sediment Rating Curves, *Journal of Geophysical*  
800 *Research: Earth Surface*, 122(10), 1901-1923, doi:10.1002/2016jf004180.

801 Vercruyssen, K., R. C. Grabowski, and R. J. Rickson (2017), Suspended sediment  
802 transport dynamics in rivers: Multi-scale drivers of temporal variation, *Earth-Science*  
803 *Reviews*, 166, 38-52, doi:10.1016/j.earscirev.2016.12.016.

804 Vrieling, A. (2006), Satellite remote sensing for water erosion assessment: A review,  
805 *Catena*, 65(1), 2-18, doi:10.1016/j.catena.2005.10.005.

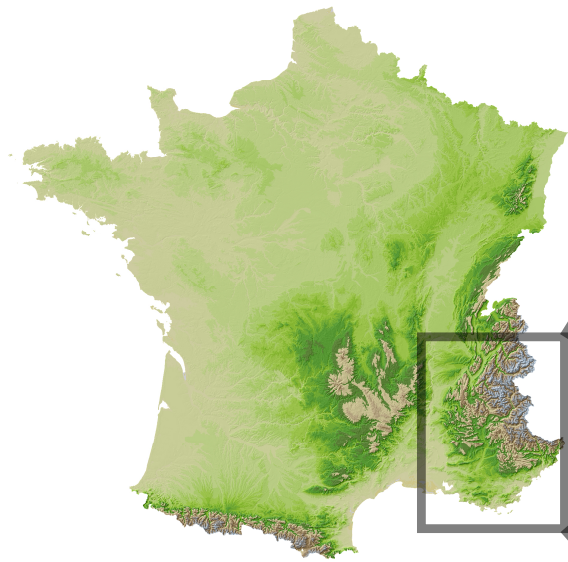
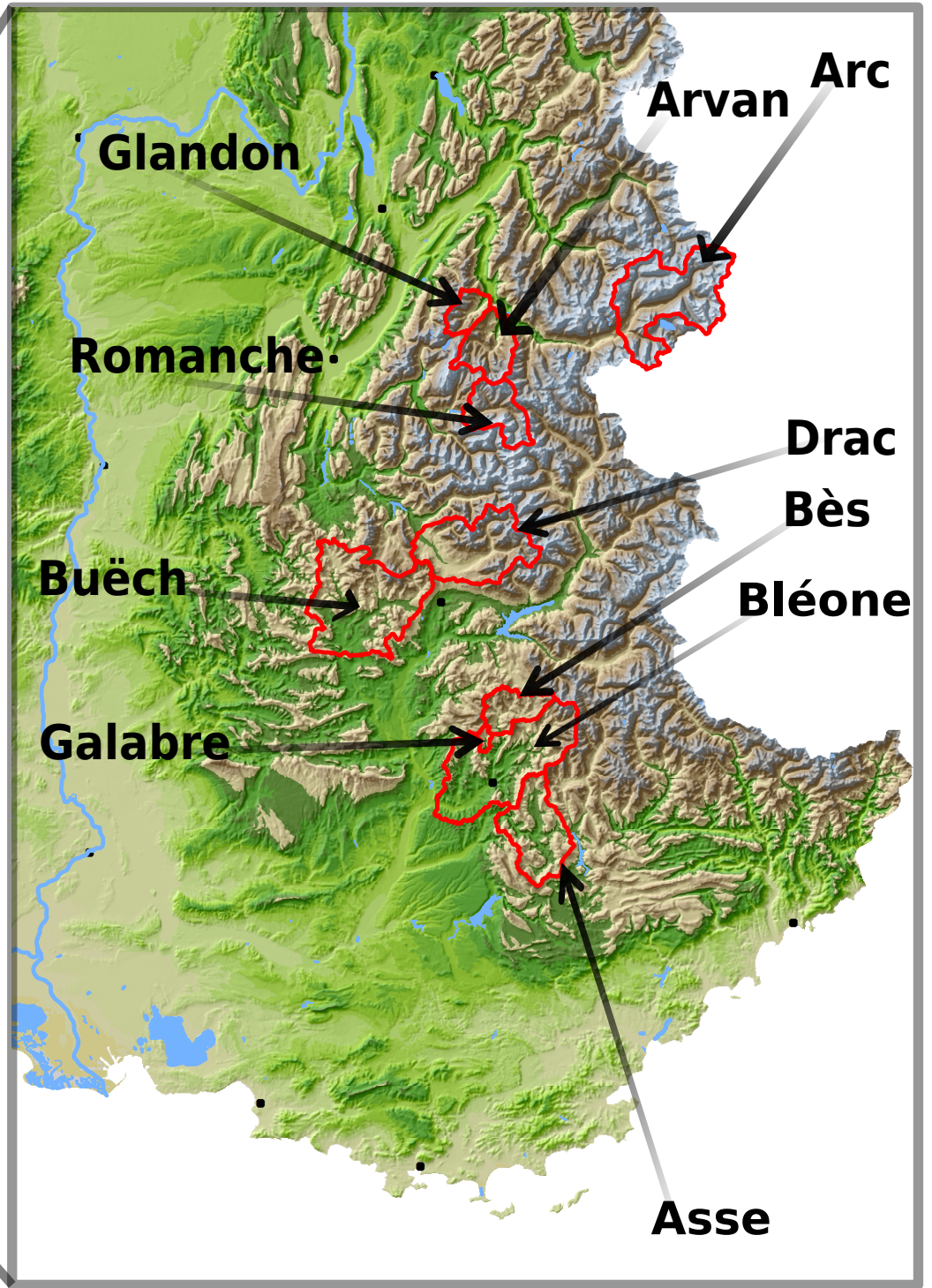
806 Walling, D. E., P. N. Owens, J. Cartera, G. J. L. Leeks, S. Lewis, A. A. Meharg, and J.  
807 Wright (2003), Storage of sediment-associated nutrients and contaminants in river  
808 channel and floodplain systems, *Applied Geochemistry*, 18(2), 195-220,  
809 doi:10.1016/S0883-2927(02)00121-X.

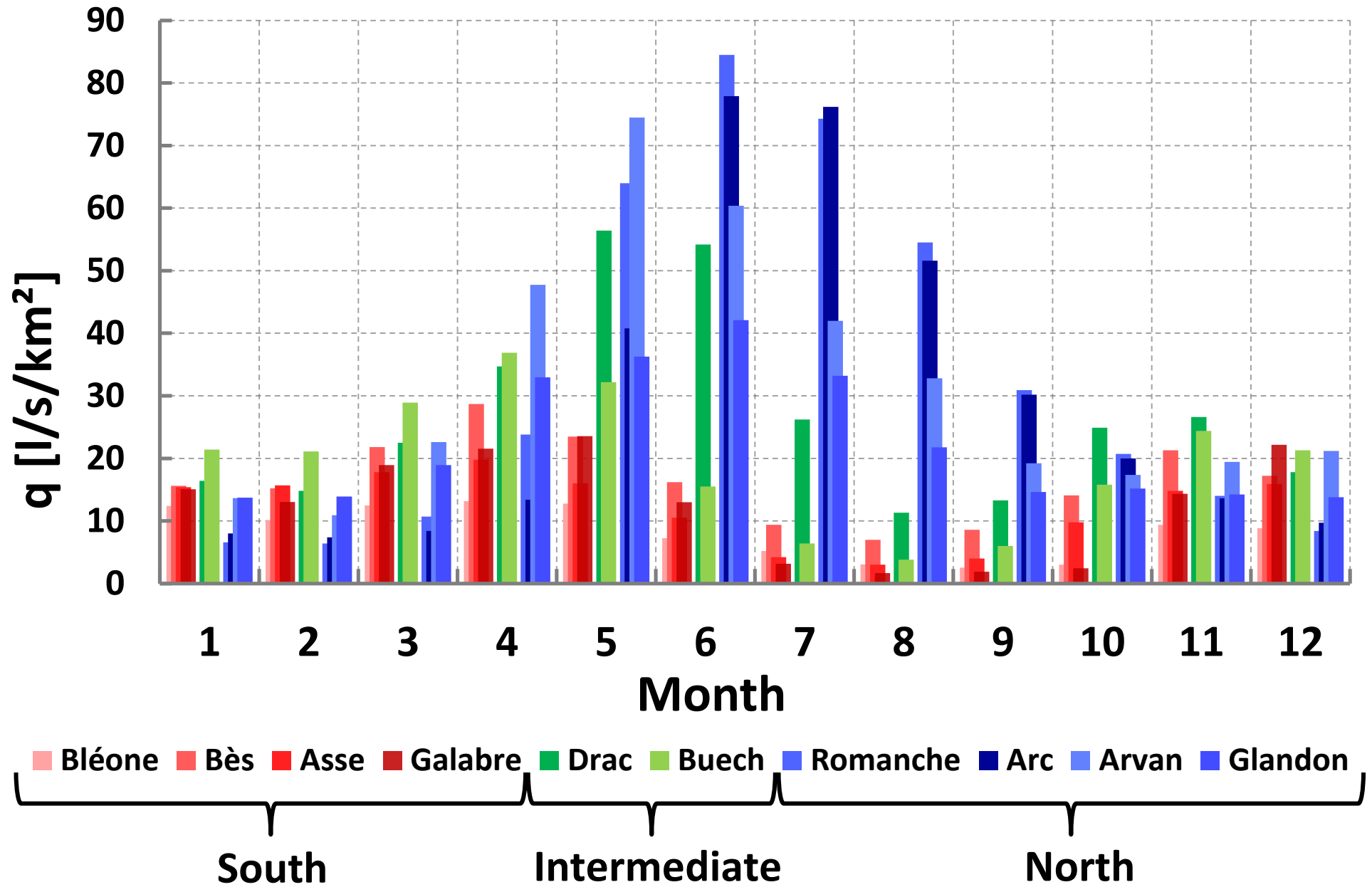
810 Williams, G. P. (1989), Sediment concentration versus water discharge during single  
811 hydrologic events in rivers, *Journal of Hydrology*, 111, 89-106, doi:10.1016/0022-  
812 1694(89)90254-0.

813 Wohl, E. (2017), Connectivity in rivers, *Progress in Physical Geography*, 41(3), 345-362,  
814 doi:10.1177/0309133317714972.

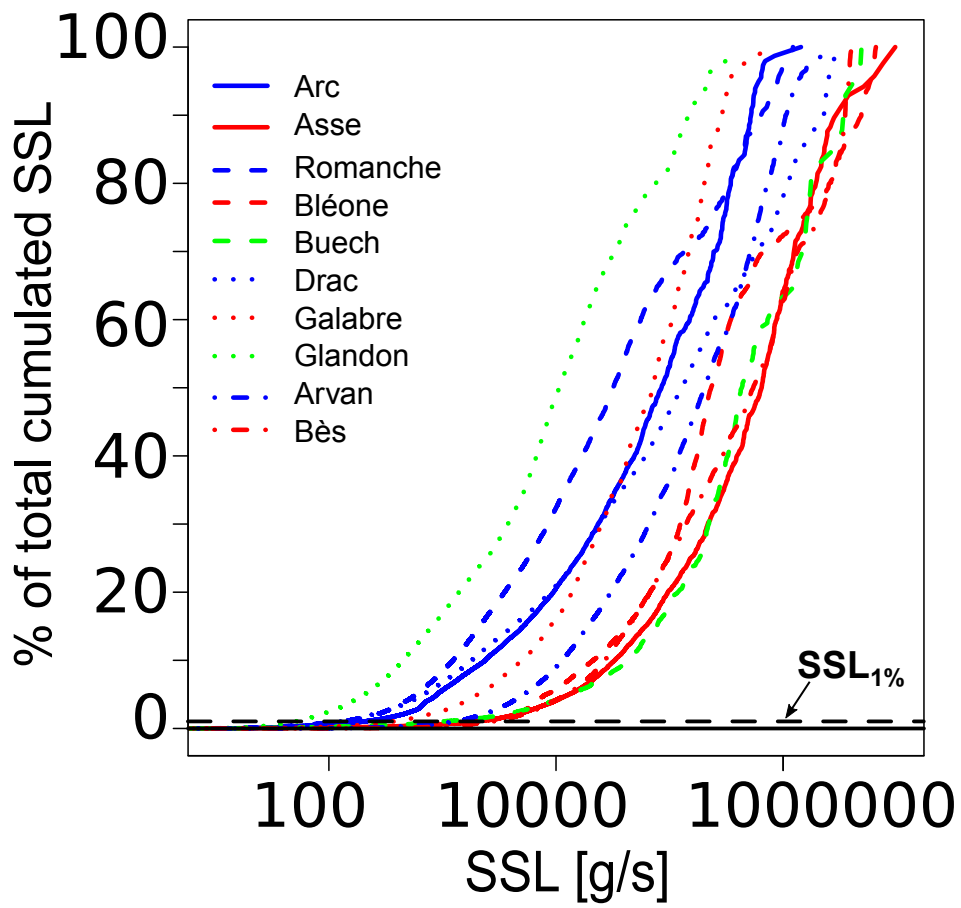
815 Zuecco, G., D. Penna, M. Borga, and H. J. van Meerveld (2016), A versatile index to  
816 characterize hysteresis between hydrological variables at the runoff event timescale,  
817 *Hydrological Processes*, 30(9), 1449-1466, doi:10.1002/hyp.10681.

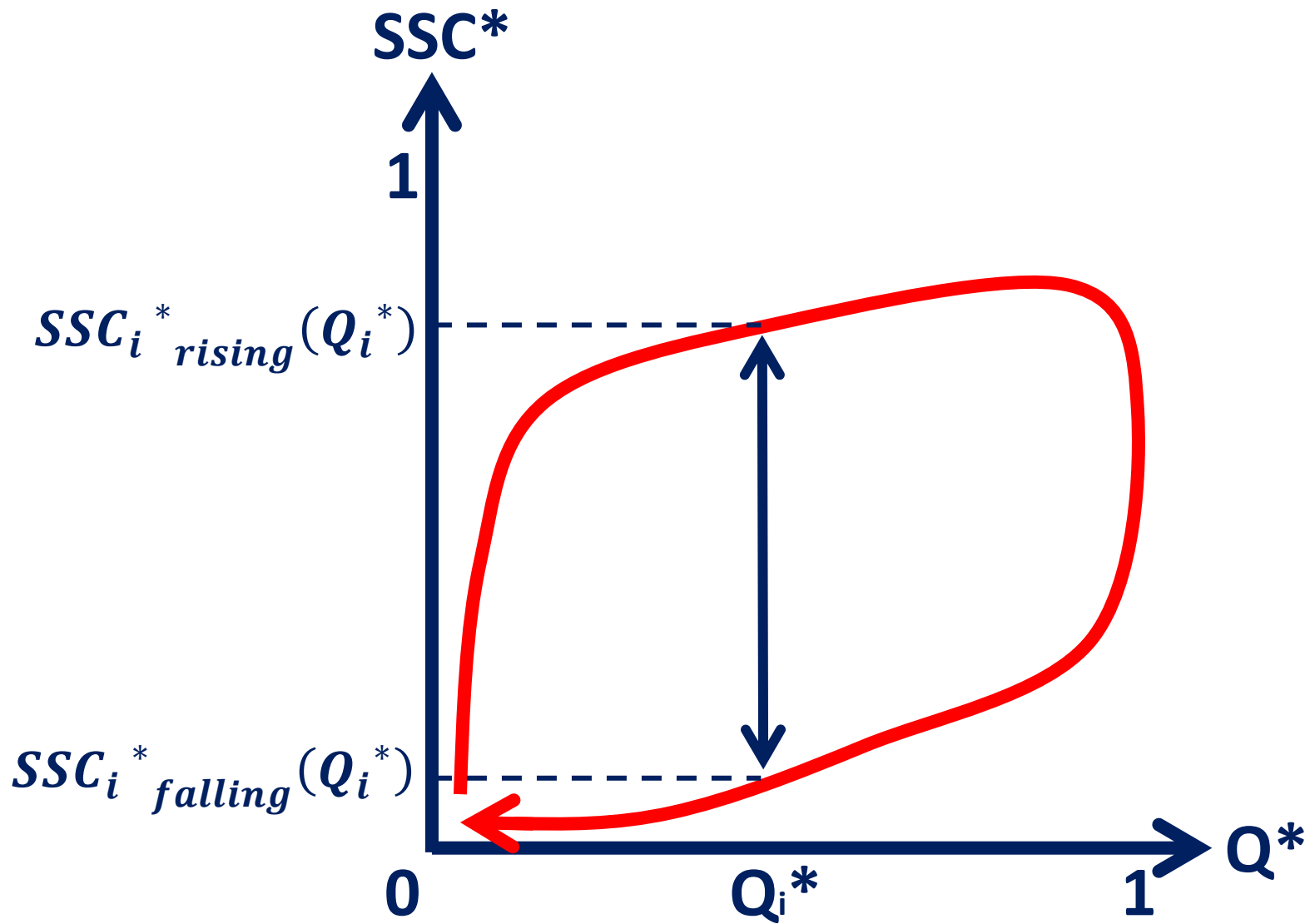
818

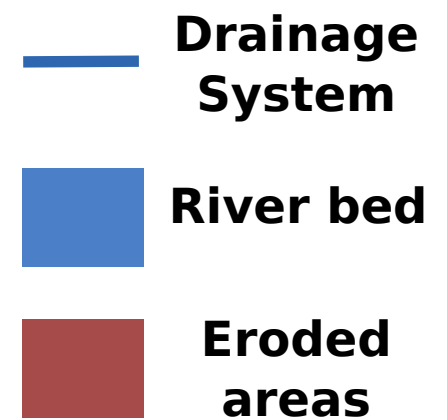
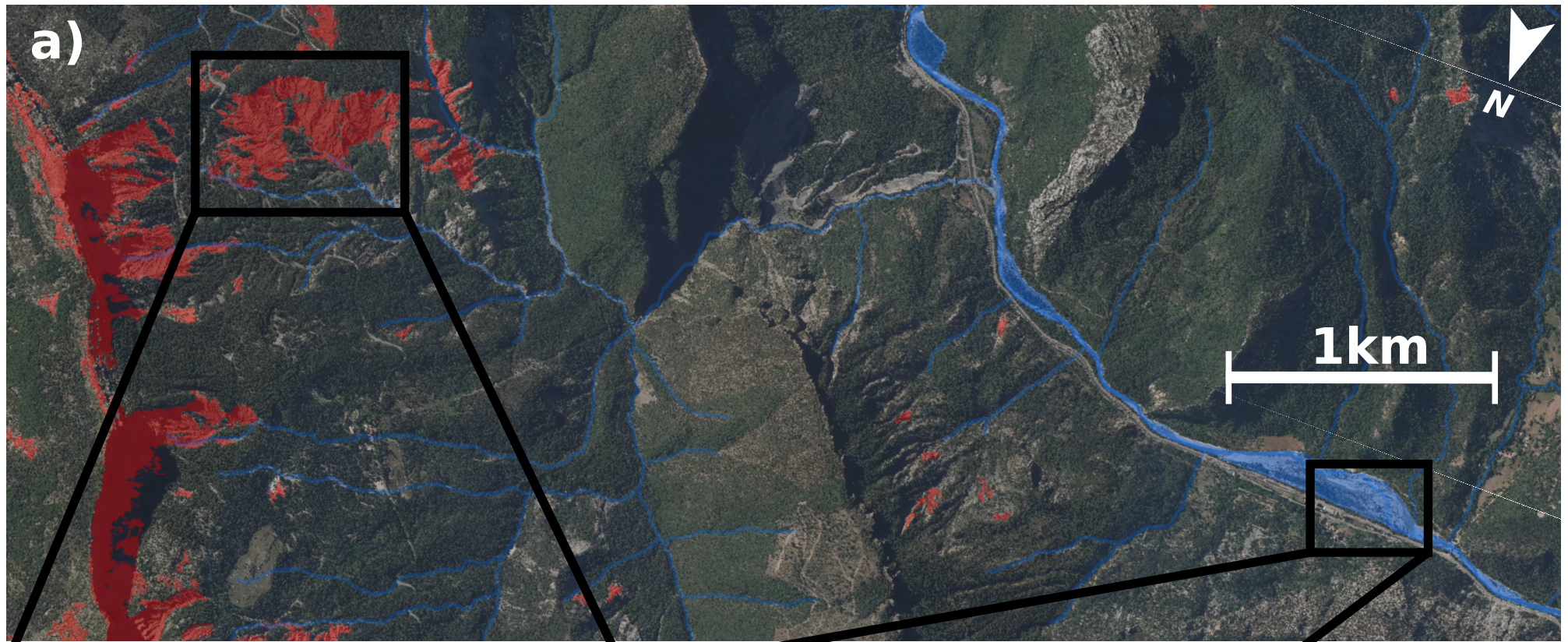








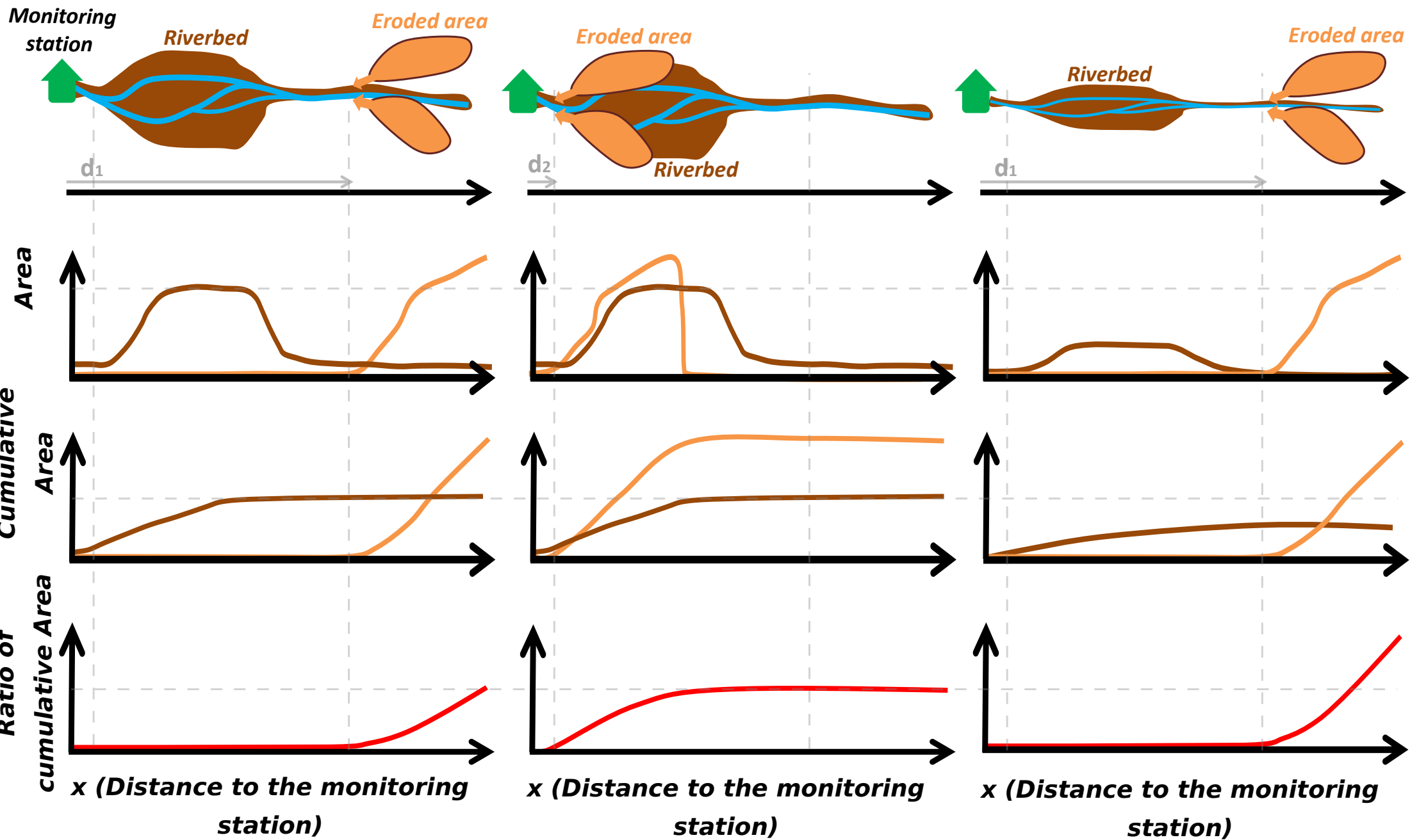


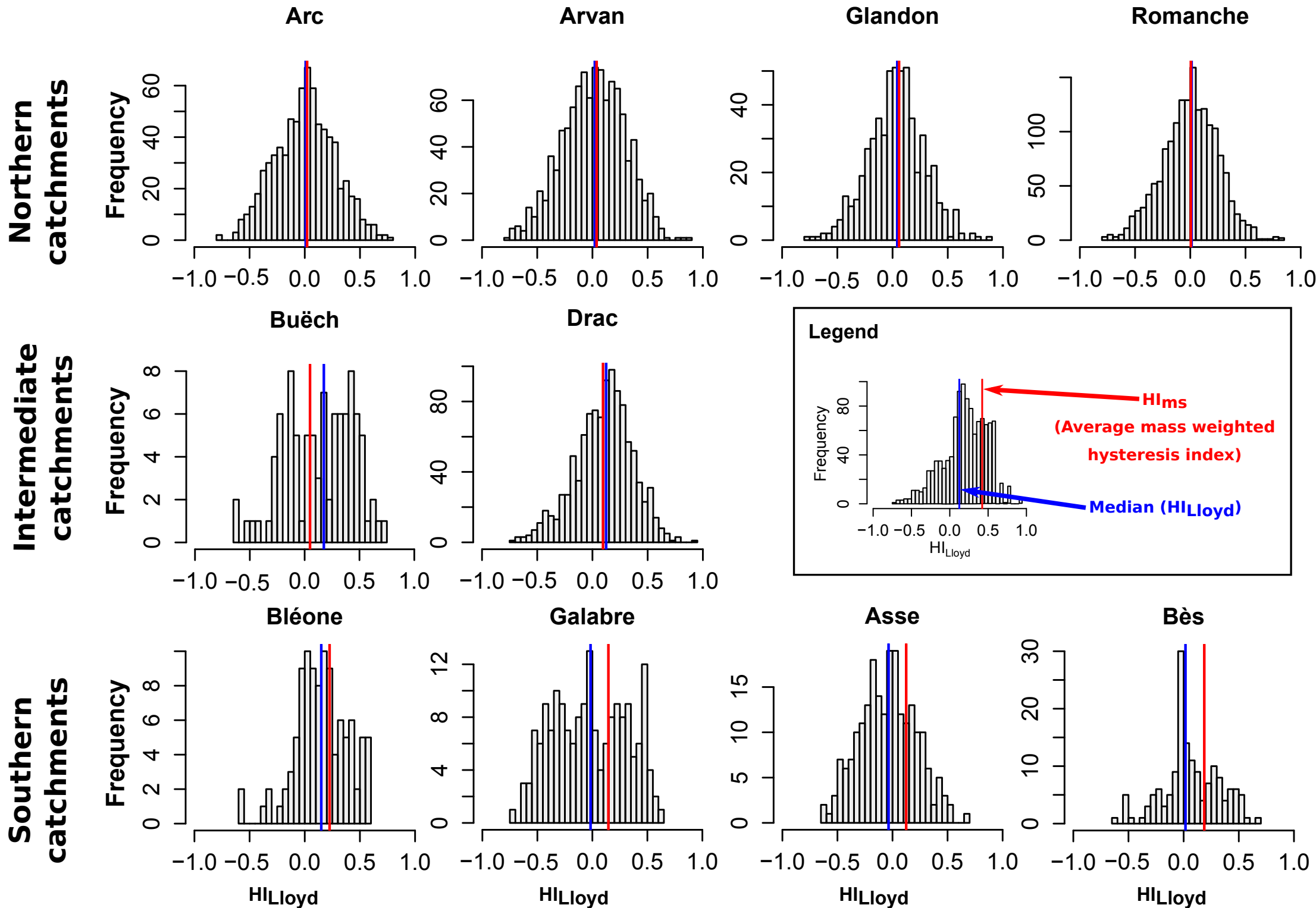


# Case (a)

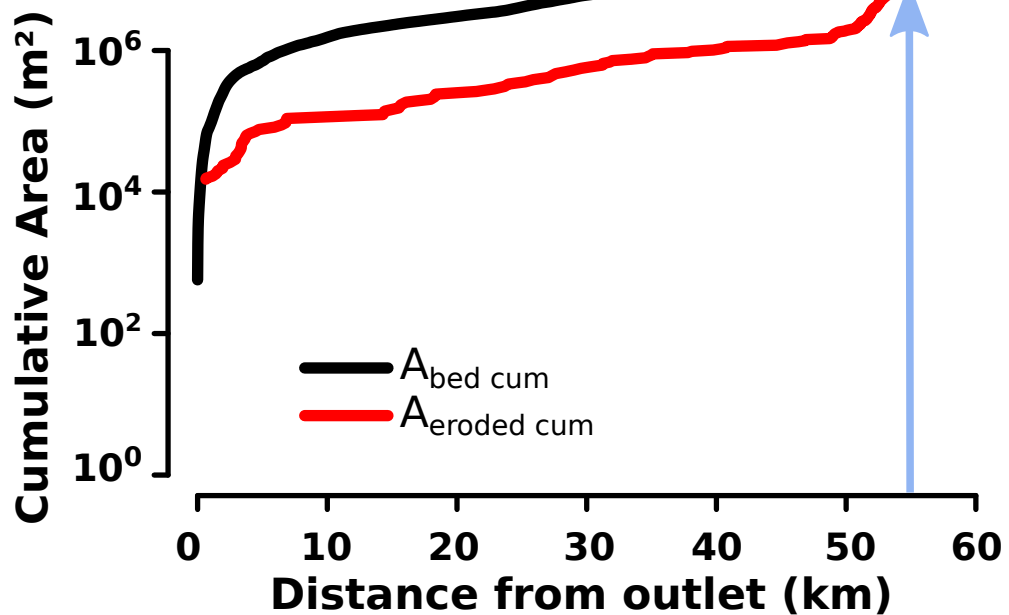
# Case (b)

# Case (c)

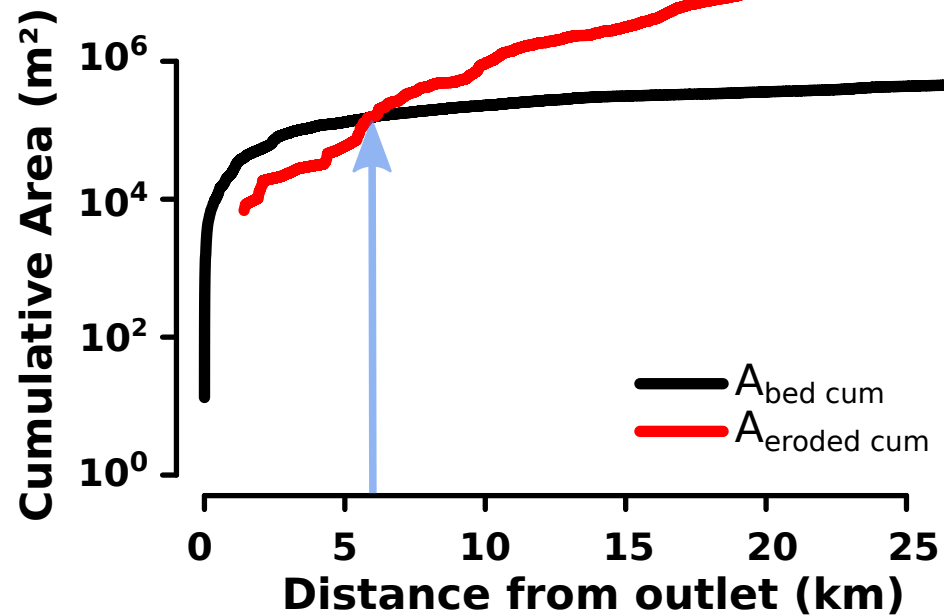


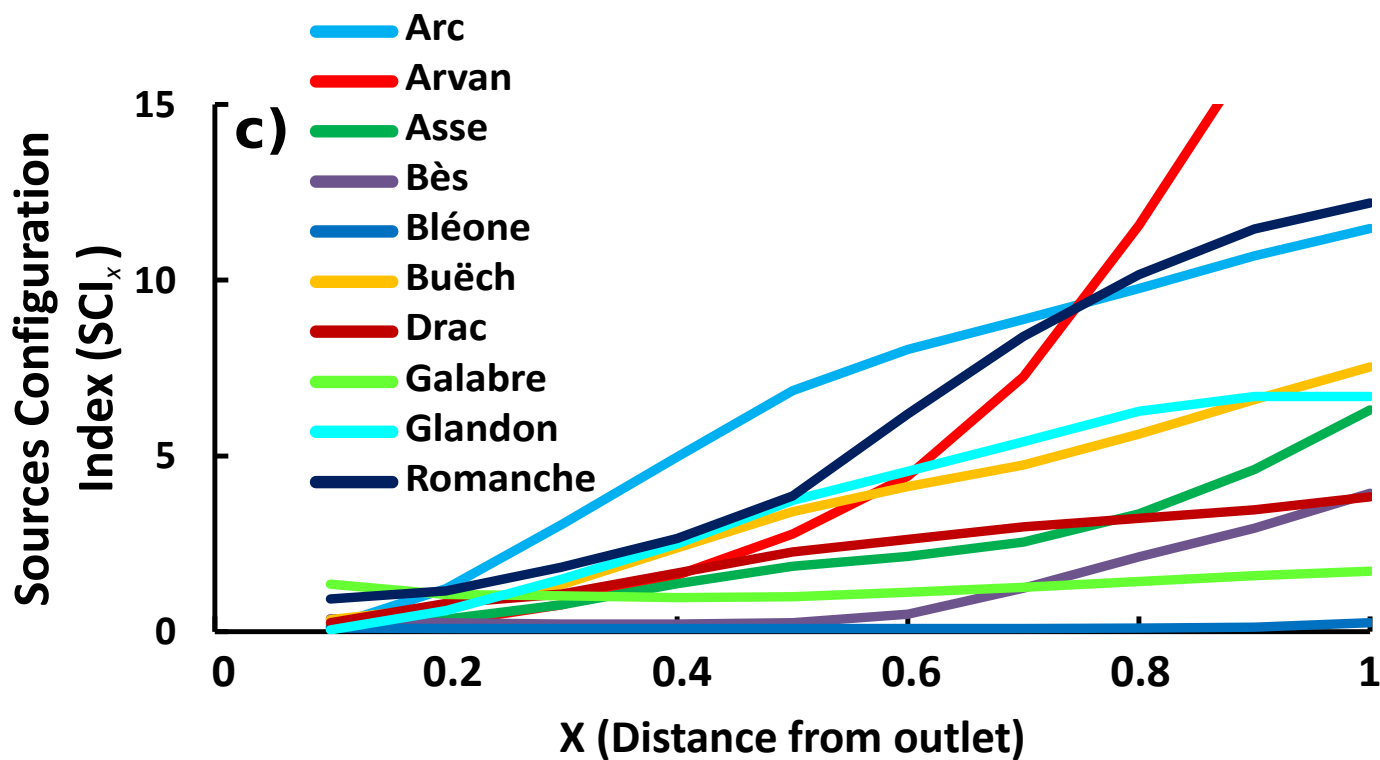
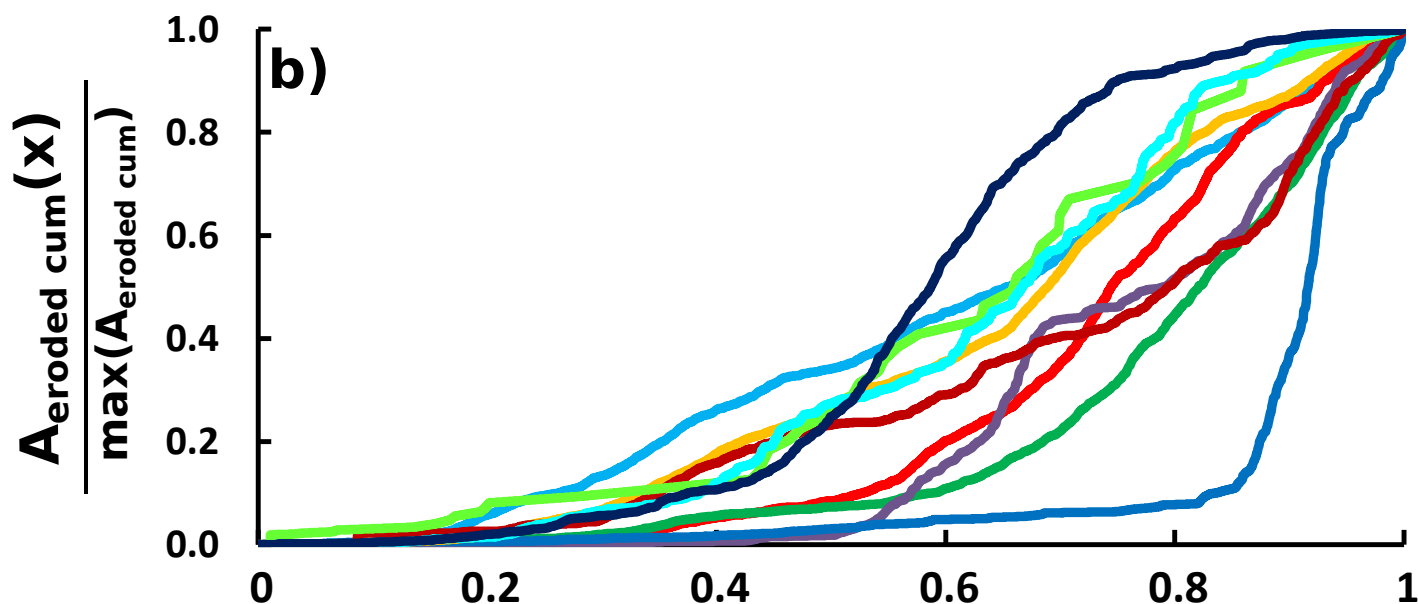
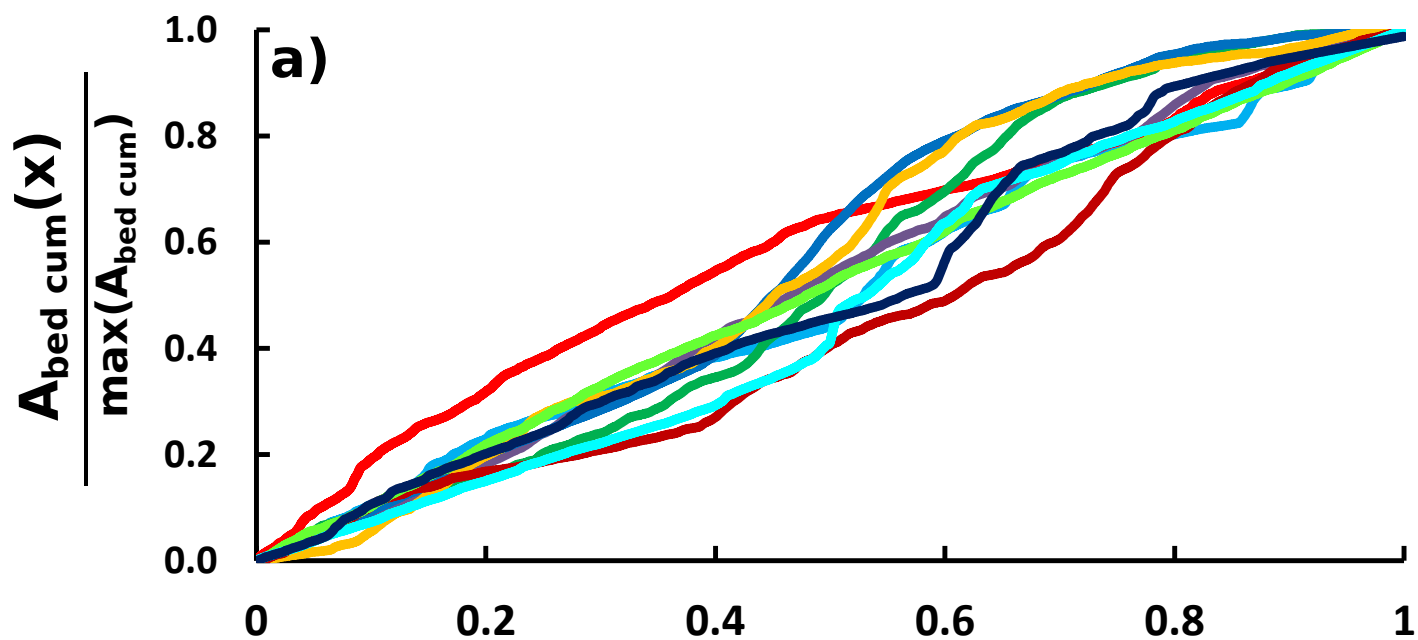


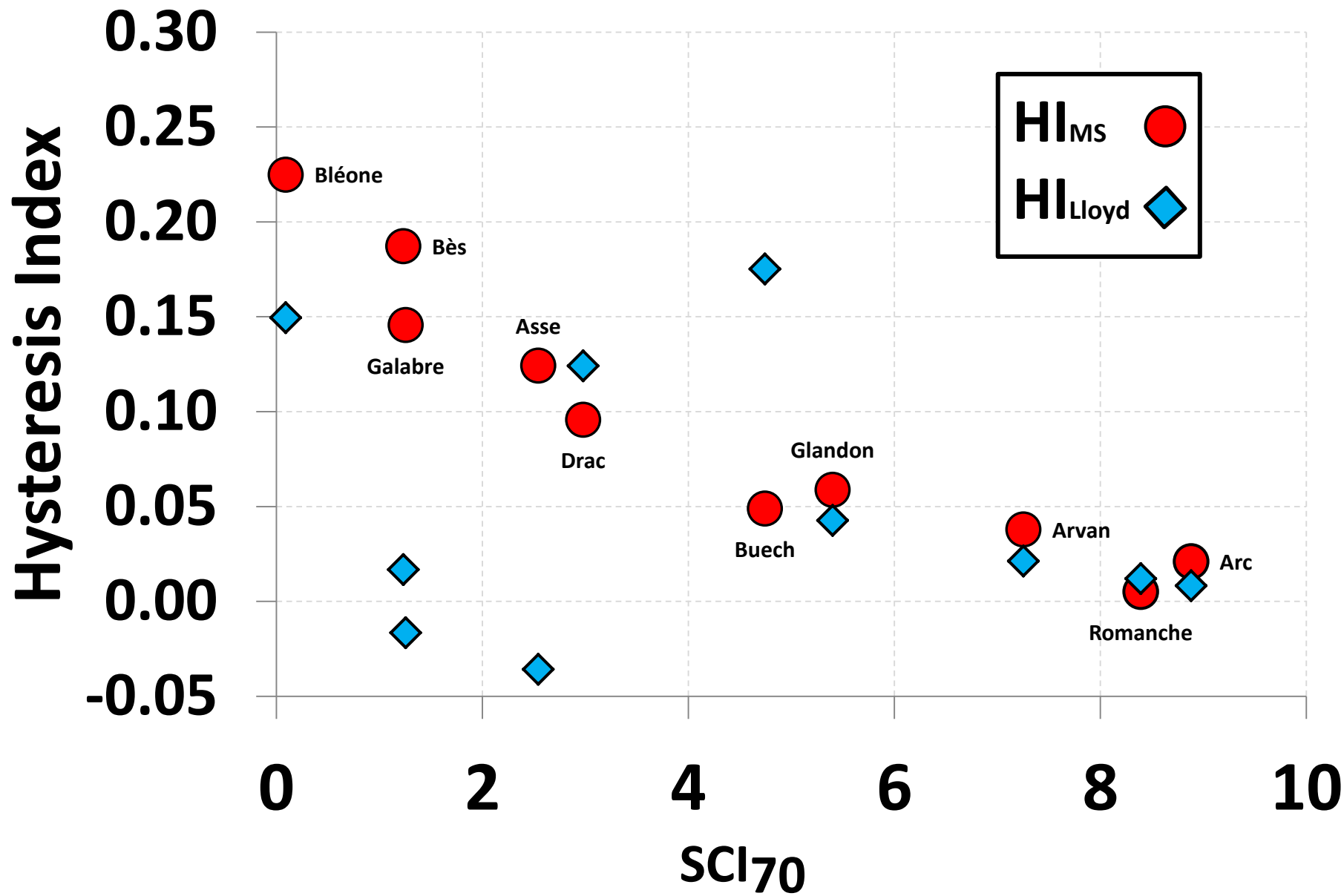
**a) Bléone**



**b) Arvan**



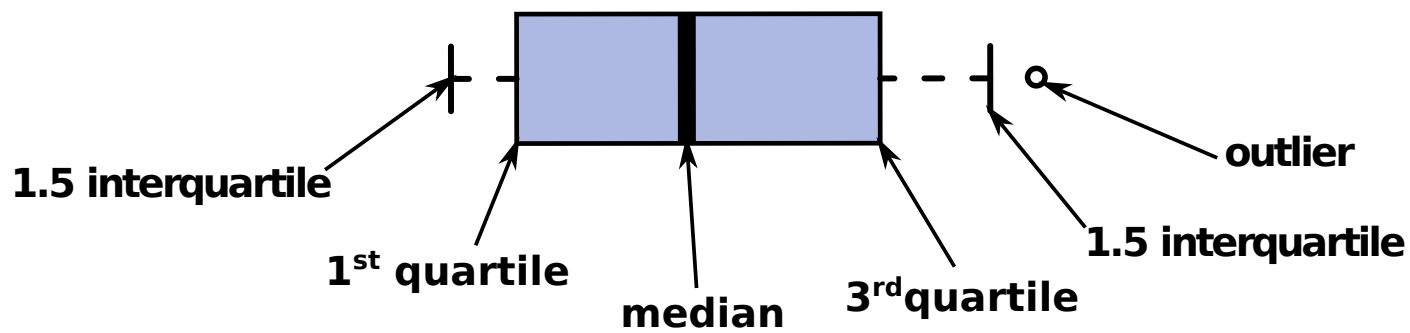
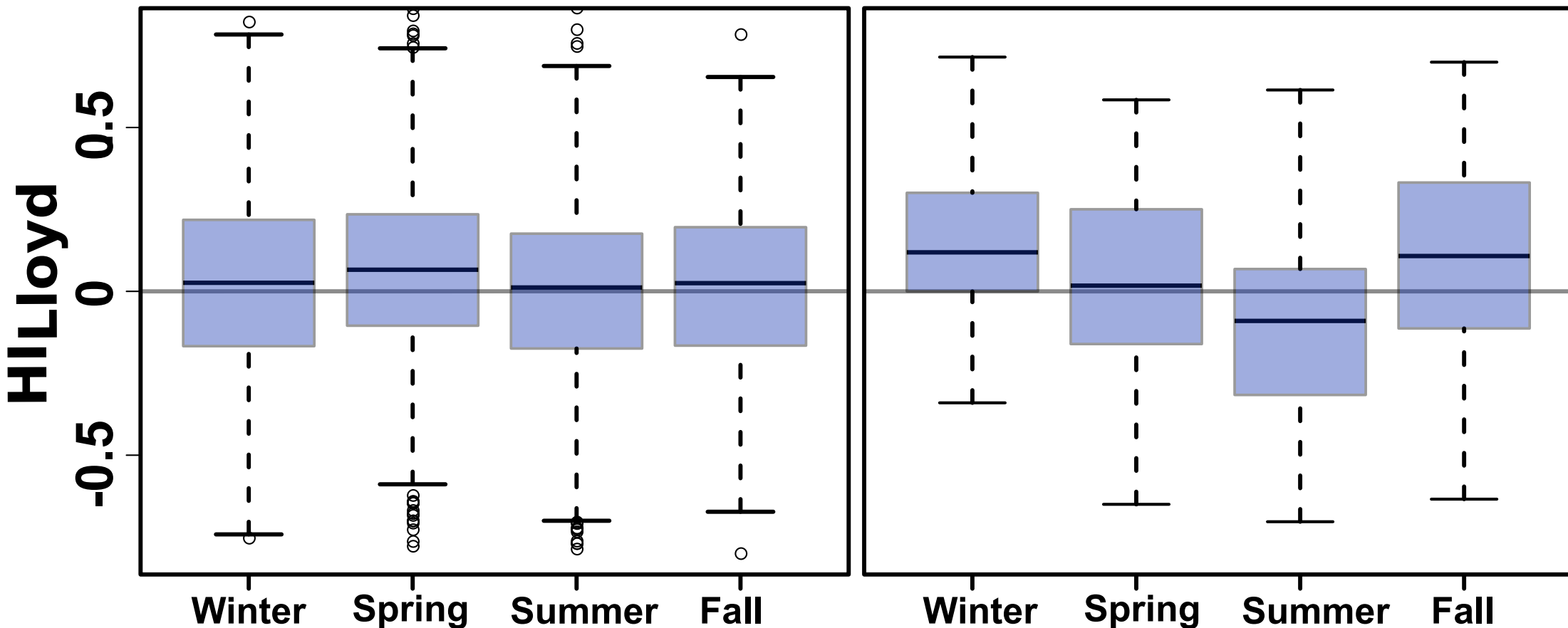


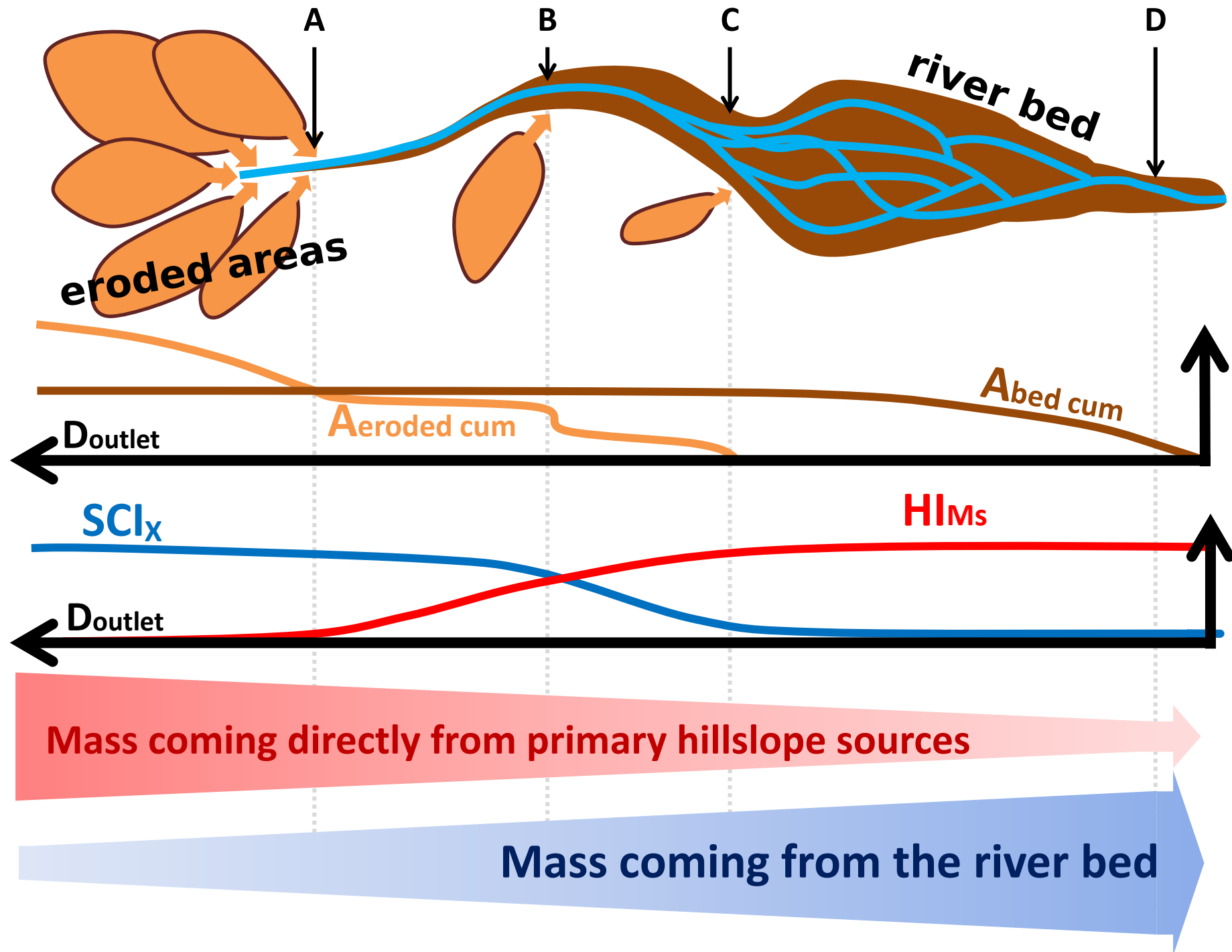




### Northern catchments

### Southern catchments





<b>Basins</b>	<b>A</b>	<b>No</b>	<b>Fo</b>	<b>Gl</b>	<b>SCR</b>	<b>HR</b>	<b>RR</b>	<b>W<sub>10</sub></b>	<b>S<sub>10</sub></b>	<b>q</b>	<b>Period</b>
<b>names</b>	<b>[km<sup>2</sup>]</b>	<b>[%]</b>	<b>[%]</b>	<b>[%]</b>	<b>[%]</b>	<b>[%]</b>	<b>[%]</b>	<b>[m]</b>	<b>[%]</b>	<b>[l/s/km<sup>2</sup>]</b>	
Arc	635	49	11	9	0	64	36	33	1.12	30	2012 - 2016
Arvan	220	24	18	2	38	61	1	22	5.92	32	2011 - 2015
Asse	375	10	41	0	9	70	21	28	0.87	12	2011 - 2016
Bès	165	14	43	0	42	46	11	20	2.57	17	2007 - 2013
Bléone	896	14	41	0	19	68	11	162	0.82	8	2007 - 2009
Buech	723	12	47	0	83	1	12	118	0.81	19	2015 - 2017
Drac	510	35	20	0	32	34	18	60	1.01	27	2007 - 2016
Galabre	22	19	11	0	39	61	0	8	8.86	13	2007 - 2013
Glandon	110	31	28	2	0	57	43	8	5.80	23	2011 - 2016
Romanche	230	51	4	12	25	33	42	14	4.17	33	2007 - 2016

**Table 1: Main catchment characteristics. Catchment size (A), no/low vegetation cover (No), forest cover (Fo), glacier cover (Gl), soft coherent rocks (SCR), heterogeneous rocks (HR), resistant rocks (RR), mean annual specific discharge (q), median active channel width calculated for the first 10 km (W<sub>10</sub>), mean slope of the river bed calculated for approximately the first 10 km (S<sub>10</sub>).**

River	SSL <sub>1%</sub> [g/s]	SSC <sub>1%</sub> [mg/l]	t <sub>exceed</sub> [h]	number of event
Arc	199	23	8	758
Arvan	1252	330	8	1048
Asse	1877	311	8	217
Bès	2677	868	8	155
Bleone	2000	181	12	104
Buech	960	104	8	94
Drac	125	14	12	1076
Galabre	360	1215	4	179
Glandon	50	21	8	561
Romanche	125	26	6	1656

**Table 2: Runoff event characteristics. (SSL<sub>1%</sub>) corresponds to the threshold of SSL below which 1% of the cumulated suspended sediment fluxes were transported, (SSC<sub>1%</sub>) corresponds to the threshold of SSC below which 1% of the cumulated suspended sediment fluxes were transported, t<sub>exceed</sub> corresponds to the minimum time step for which a valid SSL peak should exceed all following and preceding values.**

River	Mass transported			Number of events			Indexes		
	MS <sub>cl</sub> [%]	MS <sub>ccl</sub> [%]	MS <sub>no/complex</sub> [%]	Nb <sub>cl</sub> [%]	Nb <sub>ccl</sub> [%]	Nb <sub>no/complex</sub> [%]	median(HI <sub>Lloyd</sub> )	Sd(HI <sub>Lloyd</sub> )	HI <sub>MS</sub>
Arc	26	32	42	30	32	37	0.01	0.27	0.02
Arvan	34	28	38	34	30	36	0.02	0.28	0.04
Asse	58	11	31	23	31	47	-0.04	0.25	0.12
Bès	58	4	38	38	15	47	0.02	0.26	0.19
Bleone	84	2	14	60	11	30	0.15	0.24	0.22
Buech	41	31	28	62	19	19	0.18	0.31	0.05
Drac	41	24	35	43	16	41	0.12	0.26	0.10
Galabre	53	21	26	37	41	22	-0.02	0.33	0.15
Glandon	44	22	34	38	28	34	0.04	0.25	0.06
Romanche	25	28	47	28	28	43	0.01	0.25	0.01

**Table 3: Results of hysteresis analysis between SSC and Q. The percentage of the mass transported with a given hysteresis shape (Ms), the percentage of events with a given shape (Nb), and the mean, standard deviation (sd) of the Lloyd hysteresis index (HI<sub>Lloyd</sub>) were calculated as well as the average mass weighted hysteresis index (HI<sub>MS</sub>). cl : clockwise hysteresis, ccl : counterclockwise hysteresis, no/complex : no or complex hysteresis.**

	General catchment characteristics		River bed area configuration		Eroded area configuration		River bed and eroded area configuration				
	$HI_{MS}$	$HI_{Lloyd}$ median	$HI_{MS}$	$HI_{Lloyd}$ median	$HI_{MS}$	$HI_{Lloyd}$ median	$HI_{MS}$	$HI_{Lloyd}$ median			
<b>S<sub>10</sub></b>	-0.19	<b>-0.44</b>	<b>BAI<sub>10</sub></b>	0.10	<b>-0.45</b>	<b>EAI<sub>10</sub></b>	0.32	0.02	<b>SCI<sub>10</sub></b>	-0.01	-0.35
<b>W<sub>10</sub></b>	0.12	<b>0.56</b>	<b>BAI<sub>30</sub></b>	0.13	<b>-0.13</b>	<b>EAI<sub>30</sub></b>	<b>-0.26</b>	-0.08	<b>SCI<sub>30</sub></b>	<b>-0.78</b>	-0.14
<b>A</b>	-0.05	<b>0.47</b>	<b>BAI<sub>50</sub></b>	0.38	-0.04	<b>EAI<sub>50</sub></b>	<b>-0.43</b>	-0.14	<b>SCI<sub>50</sub></b>	<b>-0.94</b>	-0.07
<b>No</b>	<b>-0.63</b>	-0.08	<b>BAI<sub>70</sub></b>	0.37	0.25	<b>EAI<sub>70</sub></b>	<b>-0.71</b>	-0.22	<b>SCI<sub>70</sub></b>	<b>-0.98</b>	-0.13
<b>Fo</b>	<b>0.54</b>	<b>0.49</b>	<b>BAI<sub>90</sub></b>	0.35	0.22	<b>EAI<sub>90</sub></b>	<b>-0.71</b>	-0.25	<b>SCI<sub>90</sub></b>	<b>-0.93</b>	-0.10

1 Table 4: Spearman correlation coefficients between hysteresis indexes considering the frequency of event  
2 with a given hysteresis (median value of the Lloyd index,  $HI_{Lloyd}$ ) or the mass transported with a given  
3 hysteresis (average mass weighted hysteresis index,  $HI_{MS}$ ) and catchment characteristics:  $S_{10}$  is the mean  
4 river bed slope calculated for the first 10 km,  $W_{10}$  is the median active width calculated for the first 10 km,  $A$  is  
5 the catchment size,  $No$  is the percentage of the catchment having no or low vegetation cover, and  $Fo$  is the  
6 forest cover,  $BAI_x$  is the mean ratio of cumulated river bed area over total cumulated river bed area  
7 considering a length  $x$  upstream of the station,  $EAI_x$  is the mean ratio of cumulated eroded area over total  
8 cumulated eroded area considering a length  $x$  upstream of the station and  $SCI_x$  is the mean ratio of  
9 cumulated eroded area over cumulated bed area considering a length  $x$  upstream of the station. Bold values  
10 are significant with a confidence interval of 95% ( $p_{value} < 0.01$ ).

11